ANGELHY

Innovative solutions for design and strengthening of telecommunications and transmission lattice towers using large angles from high strength steel and hybrid techniques of angles with FRP strips

WORK PACKAGE 4 – DELIVERABLE 4.3

Finalized safety factors and formula constants

Validated design rules for single angle members

Coordinator:

National Technical University of Athens - NTUA, Greece

Beneficiaries:

Arcelormittal Belval & Differdange SA - AMBD, Luxembourg

Université de Liège – ULG, Belgium

Cosmote Kinites Tilepikoinonies AE - COSMOTE, Greece

Centre Technique Industriel de la Construction Métallique – CTICM, France

Sika France SAS - Sika France, France

AUTHORS:

UNIVERSITE DE LIEGE

Faculty of Applied Sciences, ArGEnCo Department

Quartier Polytech 1, Allée de la Découverte, 9, B52/3, 4000 Liège, Belgium

Authors: Marios-Zois Bezas, Jean-Pierre Jaspart, Jean-François Demonceau

NATIONAL TECHNICAL UNIVERSITY OF ATHENS

Institute of Steel Structures

Iroon Polytechniou 9,15780 Athens, Greece

Authors: Ioannis Vayas

ANGELHY – Innovative solutions for design and strengthening of telecommunications **Page 3**
and transmission lattice towers using large angles from high strength steel and hybrid
techniques of angles with FRP strips

TABLE OF CONTENTS

ANGELHY – Innovative solutions for design and strengthening of telecommunications   **Page 4**
and transmission lattice towers using large angles from high strength steel and hybrid
techniques of angles with FRP strips

1 Introduction and notation

In task 2.2 of Work Package WP2 of the ANGELHY project, a set of design formulae for the classification of cross-sections as well as for the prediction of the resistance of cross-sections and the stability of members made of equal leg hot-rolled angle profiles has been presented. The aim of this deliverable is to validate and improve where it is necessary the here above-mentioned set of formulae through numerical parametrical studies. For the validation of the classification system, 176 numerical analyses have been performed in total, while for the member resistances the number of the analyses came up to 220.

Furthermore, a design model and an analytical formula for the evaluation of the critical load of the segment instability observed in towers (task 1.2 of WP1) is presented and also validated through numerical studies. A way to evaluate the ultimate resistance on the basis of the critical one is also provided in the report.

The notations for the geometrical, material and other properties follow those given in EN 1993-1-1 [1]. Figure 1.1 illustrates the notations for the geometrical properties, the geometrical axes as well as the principal axes.

G   centre of gravity
h,t   geometrical properties (c=h-t-r)
u-u major principal axis or weak axis
v-v minor principal axis or strong axis
y,z geometrical axes
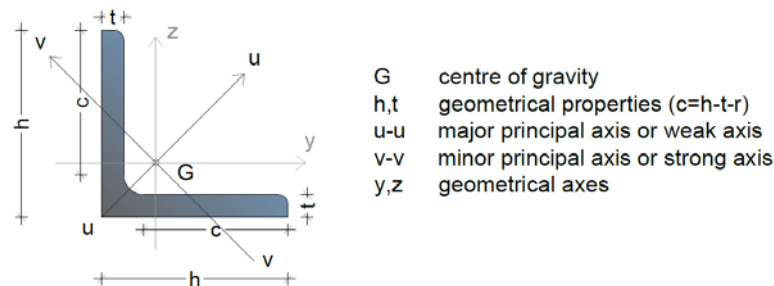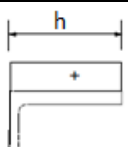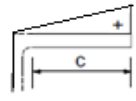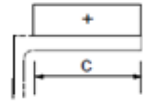
Figure 1.1: Notations for geometrical properties and principal axes
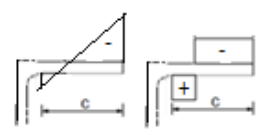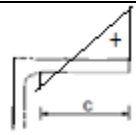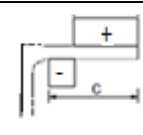
2 Classification system for angle cross-sections

2.1 Proposed classification system

Table 2.1 presents the proposed classification limits for equal leg angle cross-sections, as defined in [2].

Table 2.1: Proposed classification system for equal leg angle cross-sections

	Comment	Class 3	Class 2
Compression N_c		$\dfrac{h}{t} \leq 14\varepsilon$	
Strong axis bending M_u		$\dfrac{c}{t} \leq 14\varepsilon$	$\dfrac{c}{t} \leq 10\varepsilon$

ANGELHY – Innovative solutions for design and strengthening of telecommunications and transmission lattice towers using large angles from high strength steel and hybrid techniques of angles with FRP strips

Page 6

Weak axis bending M_v	**Tip in tension**	$\dfrac{c}{t}$ any	
	Tip in compression	$\dfrac{c}{t} \leq 16\varepsilon$	$\dfrac{c}{t} \leq 14\varepsilon$

2.2 Numerical models

The numerical analyses for the validation of the classification system were performed with ABAQUS non-linear finite element software [3] using volume elements. The samples have been modelled as pin-ended with at least three (3) volume elements per thickness (see Figure 2.1). A thicker mesh (i.e four (4) volume elements per thickness) gives better results by 1-2%, but increases a lot the required time of the analysis, that is not desirable in combination with the high number of the planned analyses. At the extremities, fictitious end plates have been considered through a specific constraint, so as to distribute uniformly the external applied loads but also to avoid any local failure at the point of application of the load.

Figure 2.1: Sample of the 3-D model used for the numerical analyses

Figure 2.2: Material law in accordance with [4]

The finite element analyses were performed considering:

- a local leg imperfection equals to h/100 (h is the width of the cross-section), based on EN 10056-2 [4], with imperfection shape affined to the lower relevant elastic instability mode obtained through an elastic instability analysis;
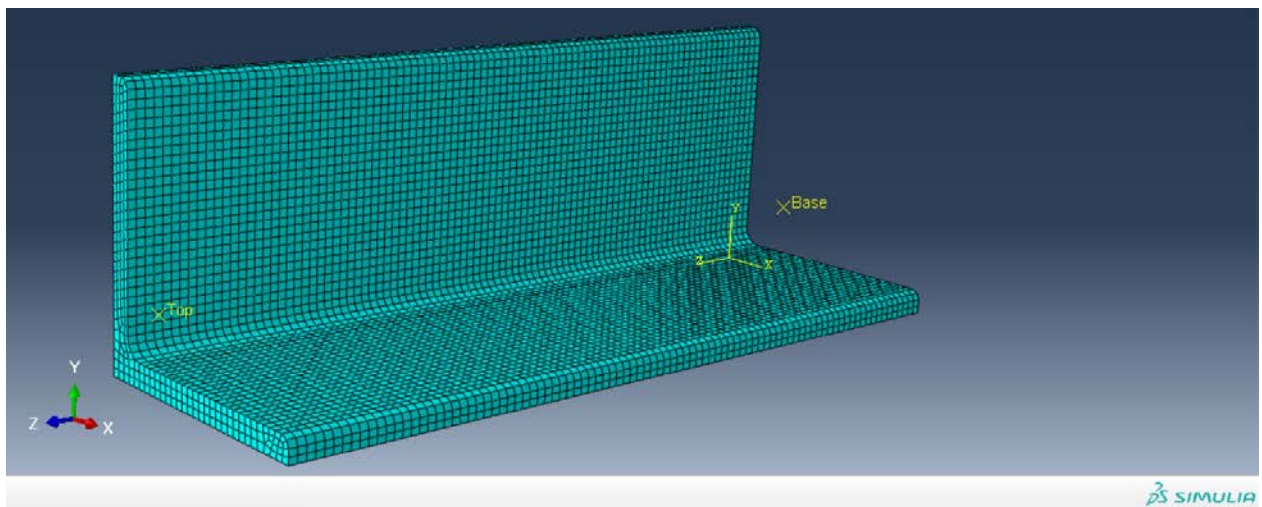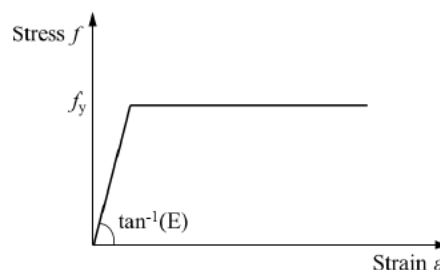- a material law without strain hardening (see Figure 2.2) in accordance with EN 1993-1-14 [5], as the objective is to check the validity of the characteristic resistances.

2.3 Cross-section under pure compression

Table 2.2 presents the cross-sections and the steel grades that have been used for the analyses in which the pin-ended samples are subjected only to an axially applied force.

Table 2.2: Details for the analyses of the cross-section under compression loading

No	Cross-Section	Steel grades
1	L45x45x3	S355 / S460 / S550 / S690
2	L45x45x4	S355 / S460 / S550 / S690
3	L70x70x5	S355 / S460 / S550 / S690
4	L70x70x6	S355 / S460 / S550 / S690
5	L250x250x17	S355 / S460 / S550 / S690
6	L250x250x20	S355 / S460 / S550 / S690
7	L250x250x22	S355 / S460 / S550 / S690
8	L250x250x26	S355 / S460 / S550 / S690

In order to prevent flexural buckling, the length of all samples has been limited by the following formula:

$$\bar{\lambda} < 0,2 \quad \Rightarrow \quad \frac{L_{cr}}{i_{min}} \cdot \frac{1}{\lambda_1} < 0,2 \quad \Rightarrow \quad L_{cr} < 18,75 \cdot \varepsilon \cdot i_{min} \quad \Rightarrow \quad \boldsymbol{L_{cr} = 18,5 \cdot \varepsilon \cdot i_{min}} \quad (2.1)$$
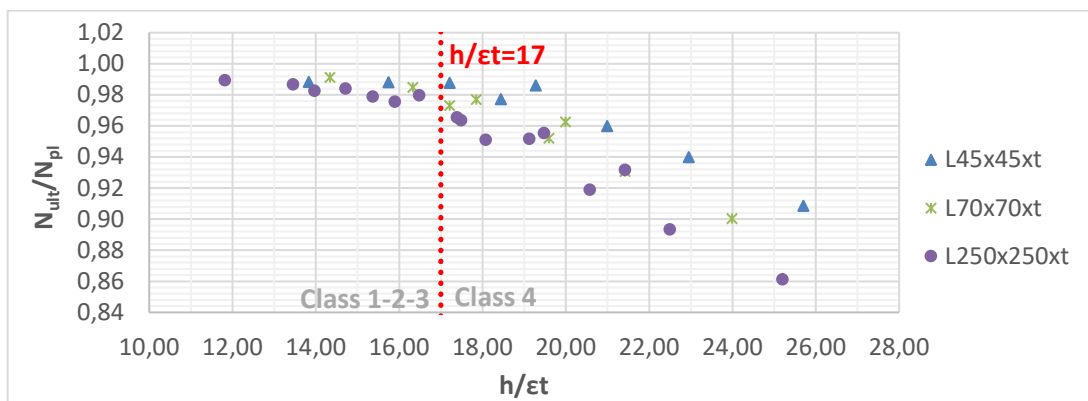
Figure 2.3: Numerical results for the CS-resistance subjected to a uniform axial load, related with the h/εt ratio

Figure 2.3 and Figure 2.4 show the ratio between the numerically obtained cross-section resistance (N_{ult}) and the plastic characteristic resistance (N_{pl}), versus the h/εt and c/εt ratio respectively. The plastic resistance of the cross-section has been evaluated by using equation (2.2).

$$N_{pl} = A \cdot f_y \quad (2.2)$$

where,

    A   is the area of the cross-section;

    f_y is the yielding stress of the material.

It can be easily observed that the scatter is bigger when the results are correlated with the $h/\varepsilon t$ ratio than the $c/\varepsilon t$ one, that makes the latter ratio more suitable.
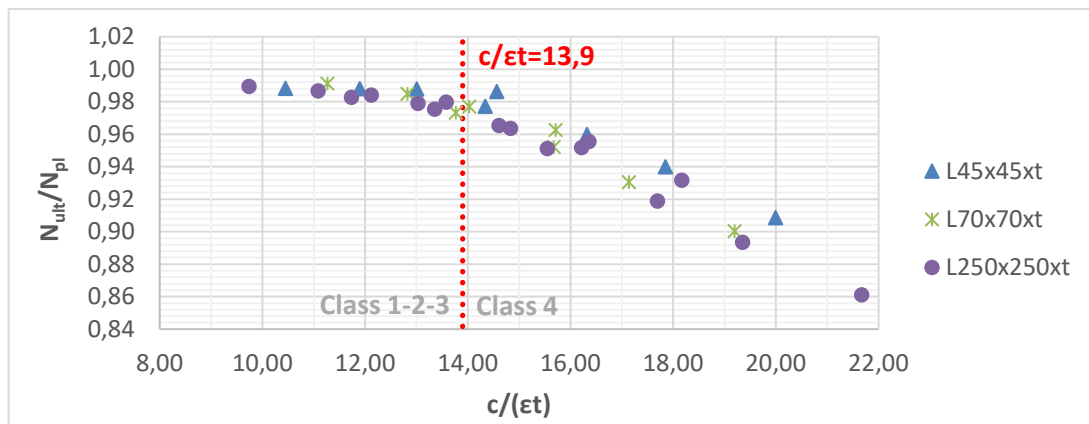

Figure 2.4: Numerical results for the CS-resistance subjected to a uniform axial load, related with the c/εt ratio

The samples that reach their plastic characteristic resistance even with a 3% deviation can be categorized as class 1. Therefore, based on the numerical results lead to the conclusion that the class-3 limit for equal leg angles subjected to compression may be set as following:

$$c/t \leq 13{,}9\varepsilon \qquad\qquad (2.3)$$

In addition, this condition:

- is in line with current provisions of Eurocode 3 and more specifically with EN 1993-1-1, table 5.2, sheet 2 for class-3 limit of outstand elements ($c/t \leq 14\varepsilon$);
- is in line with the standard EN 50341 [6], which mainly used in practice in central Europe, for the design of lattice towers made of angles ($c/t \leq 13{,}9\varepsilon$);
- is in line with the recommendations of EN 1993-3-1 [7] ($c/t \leq 13{,}9\varepsilon$), in which the c/t ratio for angles defined in EN 1993-1-1: §5.5.2 may be determined with the ratio (h-2t)/t, that is not so far from the exact value c=h-t-r.

2.4 Cross-section subjected to strong axis bending M_u

The stress distribution for strong axis bending is such that only one leg is under compression and needs classification. Table 2.3 presents the cross-sections and the steel grades that have been used for the analyses in which the pin-ended samples are subjected to strong axis bending moment M_u.

As there are no hot-rolled angle profiles with steel grade less than S690, that could give $c/\varepsilon t$ ratios higher than 25, the last 8 analyses, i.e. 15* and 16* in Table 2.3, are theoretical and are just contemplated to investigate the behaviour of the cross-section and validate the limit between class 3 and class 4.

In order to prevent lateral torsional buckling, the length of all samples has been each time adapted so as the relative slenderness remains $\lambda_{LT} \leq 0{,}4$.

Figure 2.5 shows the ratio between the numerical results for the cross-section resistance ($M_{ult,u}$) and the plastic characteristic resistance, versus the $c/\varepsilon t$ ratio, where c=h-t-r. The plastic resistance of the cross-section has been evaluated by using eq.(2.4):

$$M_{pl,u} = W_{pl,u} \cdot f_y \qquad\qquad (2.4)$$

where,

$\quad$ $W_{pl,u}$ $\quad$ is the plastic modulus about u axis and is taken equal to $1{,}5 \cdot W_{el,u}$;

$\quad$ f_y $\quad\quad$ is the yielding stress of the material.

Table 2.3: Details for the analyses of the cross-section subjected to strong axis bending M_u

No	Cross-Section	Steel grades
1	L45x45x3	S355 / S460 / S550 / S690
2	L45x45x4	S355 / S460 / S550 / S690
3	L70x70x5	S355 / S460 / S550 / S690
4	L70x70x6	S355 / S460 / S550 / S690
5	L120x120x7	S355 / S460 / S550 / S690
6	L120x120x8	S355 / S460 / S550 / S690
7	L130x130x8	S355 / S460 / S550 / S690
8	L130x130x9	S355 / S460 / S550 / S690
9	L150x150x10	S355 / S460 / S550 / S690
10	L150x150x12	S355 / S460 / S550 / S690
11	L250x250x17	S355 / S460 / S550 / S690
12	L250x250x20	S355 / S460 / S550 / S690
13	L250x250x22	S355 / S460 / S550 / S690
14	L250x250x26	S355 / S460 / S550 / S690
15*	L120x120x7	S800 / S900 / S1000 / S1100
16*	L130x130x8	S800 / S900 / S1000 / S1100

For the angle cross-section, due to its unsymmetry, the $W_{el,u}$ is different for a top fibre (at the tip) or a bottom fibre (at the toe). However, for the design of the cross-section, the most distant fibre from centroid is considered when calculating the elastic modulus (i.e at the tip of the leg), which results in higher stress calculations. In this case, the elastic modulus about u axis can be derived from the following formula:

$$W_{el,u} = \frac{I_u}{0,5h\sqrt{2}}$$
(2.5)

where,

    I_u is the moment of inertia about u axis
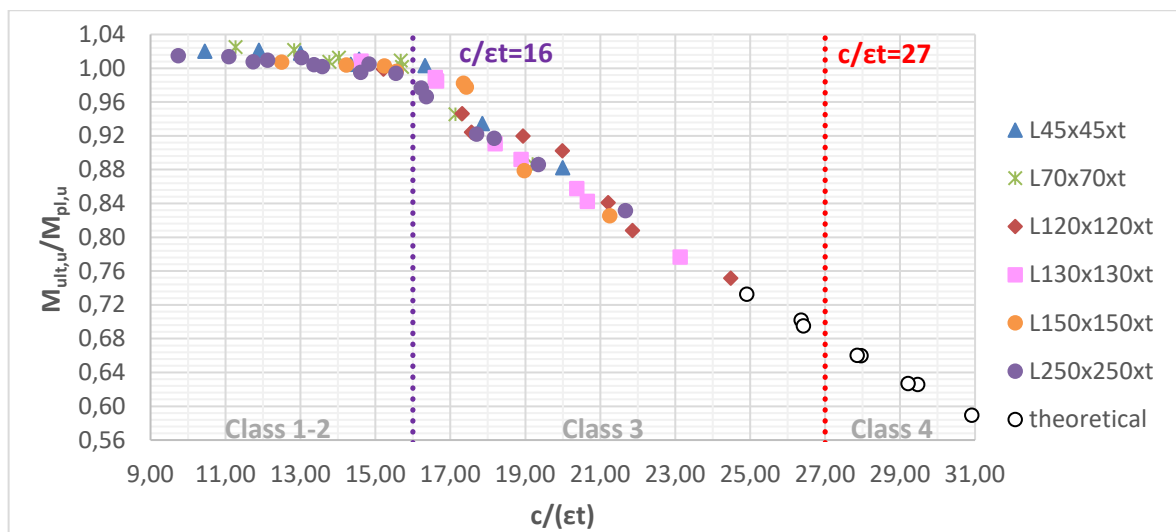
    h   is the width of the cross-section

Figure 2.5: Numerical results for the CS-resistance subjected to strong axis bending M_u, related with the c/εt ratio

ANGELHY – Innovative solutions for design and strengthening of telecommunications **Page 10**
and transmission lattice towers using large angles from high strength steel and hybrid
techniques of angles with FRP strips

The samples that reach their plastic characteristic resistance ($1,5M_{el}$) even with a 3% deviation can be categorized as class 1-2, while the class-3 limit can be easily found when $M_{ult,u}$ is equal to $M_{el,u}$ and then $M_{ult,u}/M_{pl,u} = 0,66$. Subsequently, from the numerical results, the class-2 limit for equal leg angles subjected to strong axis bending is $c/t \leq 16\varepsilon$, while the class-3 limit it can be set as $c/t \leq 27\varepsilon$.

Normatively for plastic behaviour, the leg is an outstand element subjected to uniform compression and then class-2 limit may be obtained from EN 1993-1-1, Table 5.2, sheet 2 as $c/t \leq 10\varepsilon$. The background of this value may be found in ESDEP [8] where it is indicated that a class-2 limit can be obtained by defining the value of the reduced plate slenderness $\overline{\lambda_{p,min}}$ by eq (2.6) as equal to 0,6:

$$\overline{\lambda_p} = \frac{c/t}{28,427\varepsilon\sqrt{k_\sigma}} = \overline{\lambda_{p,min}} \Rightarrow \frac{c}{t} = 17,0562\varepsilon\sqrt{k_\sigma} \tag{2.6}$$

The buckling factor is $k_\sigma = 0,43$ for simply support boundary conditions. So, a c/t value of $11,18\varepsilon$ is found (rounded to 10ε in Table 5.2, sheet 2). If clamped boundary conditions are now assumed, $k_\sigma = 1,25$ [9,10], what leads to $c/t \leq 19,07\varepsilon$. By observing the numerical and analytical results, it can be concluded that the actual class-2 limit is between the above two extreme cases and finally the following limit may be adopted:

$$\frac{c}{t} \leq 16\varepsilon \tag{2.7}$$

That defines the limit between classes 2 and 3.

For elastic behaviour, the compression leg is an outstand element subjected to a stress ratio $\psi = \frac{\sigma_2}{\sigma_1} = \frac{h-c}{h} = 0,15$. Based on EN 1993-1-1, Table 5.2, sheet 2, the class-3 limit is equal to $c/t \leq 15,4\varepsilon$ However, it seems that the leg in tension has enough stiffness to restrain the leg in compression. Thus, the corresponding buckling factor for clamped boundary conditions [9,10] is $k_\sigma = 1,57$. Then, the class-3 limit may be obtained from the general formula of EN 1993-1-1, Table 5.2, sheet 2:

$$\frac{c}{t} \leq 21\varepsilon\sqrt{1,57} = 26,3\varepsilon \tag{2.8}$$

Therefore, the class-3 limit may be kept as calculated above, that is also on the safe side in comparison to the numerical results.

2.5 Cross-section subjected to weak axis bending M_v

When the cross-section is subjected to weak axis bending, the stress conditions for the two legs are identical. Accordingly, classification refers to both legs. For this loading, two cases are defined and check afterwards:

- the tip is under compression;
- the tip is in tension.

2.5.1 Tip in compression

Table 2.4 presents the cross-sections and the steel grades that have been used for the analyses in which the pin-ended samples are subjected to weak axis bending moment M_v-tip in compression. As there are no hot-rolled angle profiles with steel grade less than S690 that give $c/\varepsilon t$ ratios more than 25, the last 8 analysis, i.e. 15* and 16* in Table 2.4, are theoretical so as to investigate the behaviour of the cross-section and validate the limit between class 3 and class 4.

ANGELHY – Innovative solutions for design and strengthening of telecommunications   **Page 11**
and transmission lattice towers using large angles from high strength steel and hybrid
techniques of angles with FRP strips

Table 2.4: Details for the analyses of the cross-section subjected to weak axis bending M_v

No	Cross-Section	Steel grades
1	L45x45x3	S355 / S460 / S550 / S690
2	L45x45x4	S355 / S460 / S550 / S690
3	L70x70x5	S355 / S460 / S550 / S690
4	L70x70x6	S355 / S460 / S550 / S690
5	L120x120x7	S355 / S460 / S550 / S690
6	L120x120x8	S355 / S460 / S550 / S690
7	L130x130x8	S355 / S460 / S550 / S690
8	L130x130x9	S355 / S460 / S550 / S690
9	L150x150x10	S355 / S460 / S550 / S690
10	L150x150x12	S355 / S460 / S550 / S690
11	L250x250x17	S355 / S460 / S550 / S690
12	L250x250x20	S355 / S460 / S550 / S690
13	L250x250x22	S355 / S460 / S550 / S690
14	L250x250x26	S355 / S460 / S550 / S690
15*	L120x120x7	S700 / S800 / S900 / S950
16*	L130x130x8	S700 / S800 / S900 / S950
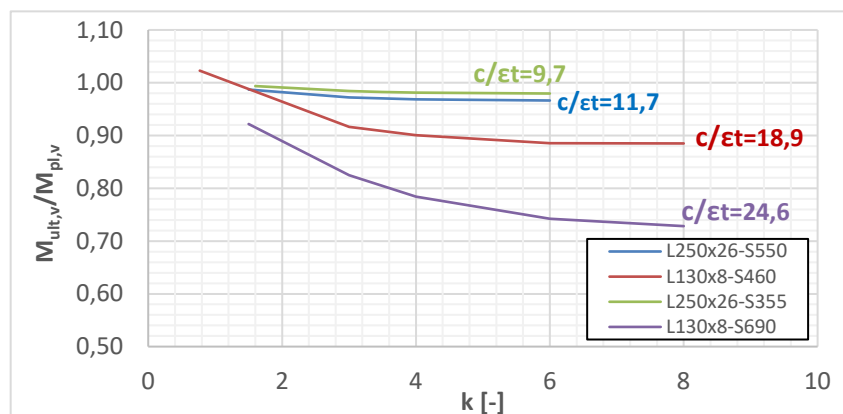
Figure 2.6: Numerical results for the CS-resistance subjected to weak axis bending M_v, related with the length parameter k

A number of numerical simulations have been performed to evaluate an optimal length value ($L=k \cdot h$), so that the yielding develops freely along the member while the cross-section resistance is independent of the length. It has been found that the value of the sample length L=6h [mm], where h is the width of the angle, is working quite well (see Figure 2.6):

- for small $c/\varepsilon t$ ratios which corresponds to class 1 or 2 profiles, the difference between L=4h and L=6h is less than 0,5%, which is acceptable.

- for big $c/\varepsilon t$ ratios which corresponds to class 3 and 4 profiles, the difference between L=6h and L=8h is less than 1,8% which is also acceptable.

The details and results of this parametric study are summarized in Table 2.5 and Figure 2.6. The calculation of $M_{pl,v}$ has been done with eq.(2.9).

Table 2.5: Details of the numerical simulations about the optimal length value

No	h [mm]	f_y [N/mm²]	t [mm]	c/εt	k	L=k·h [mm]	$M_{ult,v}$ [kNm]	$M_{pl,v}$ [kNm]	$M_{ult,v}/M_{pl,v}$
1	250	355	26	9,7	1,6	400	183,174	184,34	0,99
					3	750	181,432	184,34	0,98
					3,5	875	181,160	184,34	0,98
					4	1000	180,939	184,34	0,98
					6	1500	180,573	184,34	0,98
2	250	550	26	11,7	1,5	375	281,899	285,6	0,99
					3	750	277,566	285,6	0,97
					4	1000	276,539	285,6	0,97
					6	1500	275,984	285,6	0,97
3	130	460	8	18,89	0,77	100	21,420	20,94	1,02
					3	390	19,187	20,94	0,92
					4	520	18,863	20,94	0,90
					6	780	18,538	20,94	0,89
					8	1040	18,531	20,94	0,88
4	130	690	8	24,63	1,5	195	28,962	31,42	0,92
					3	390	25,916	31,42	0,82
					4	520	24,646	31,42	0,78
					6	780	23,319	31,42	0,74
					8	1040	22,882	31,42	0,73

Figure 2.8 shows the ratio between the numerical results for the cross-section resistance ($M_{ult,v}$) and the plastic characteristic resistance, versus the c/εt ratio, where c=h-t-r. The plastic resistance of the cross-section has been evaluated by using eq.(2.9).

$$M_{pl,v} = W_{pl,v} \cdot f_y \qquad (2.9)$$

where,

$W_{pl,v}$ is the plastic modulus about v axis;

f_y is the yielding stress of the material.

The plastic modulus about v axis have been estimated through the following equation by assuming that the radius at the toe of the cross-sections is equal to zero (r=0). The notation of the following formulas are supplemented by Figure 2.7.

$$W_{pl,v} = \frac{A}{2} \cdot (c + d) \qquad (2.10)$$

where,

A   is the area of the whole cross-section;

c   is the distance between the centre of gravity of the sub-cross-section 2 and the plastic neutral axis (pna), and it can be calculated by the equation:

$$c = \sqrt{2} \cdot \left(\frac{h_2}{2} - y_{G_3}\right) \qquad (2.11)$$

d   is the distance between the centre of gravity of the sub-cross-section 1 and the pna, and it can be calculated by the equation:

$$d = \sqrt{2} \cdot \left(y_{G_1} - \frac{h_2}{2}\right) \qquad (2.12)$$

h_2 is the width of the sub-cross-section 2 and is equal to $h_2=h-h_1$ $\qquad$ (2.13)

h_1 is the width of the sub-cross-section 1 and is equal to $h_1=A/4t$ $\qquad$ (2.14)

h   is the width of the whole cross-section

t	is the thickness of the whole cross-section
y_{G_1}	is the distance between the centre of gravity of the sub-cross-section 1 and the point O(0,0) along y' axis and it can be calculated by the equation:

$$y_{G_1} = \frac{h_1}{4} + \frac{h_2}{2} + \frac{t}{4} \tag{2.15}$$

y_{G_2}	is the distance between the centre of gravity of the sub-cross-section 2 and the point O(0,0) along y' axis and it can be calculated by the equation:

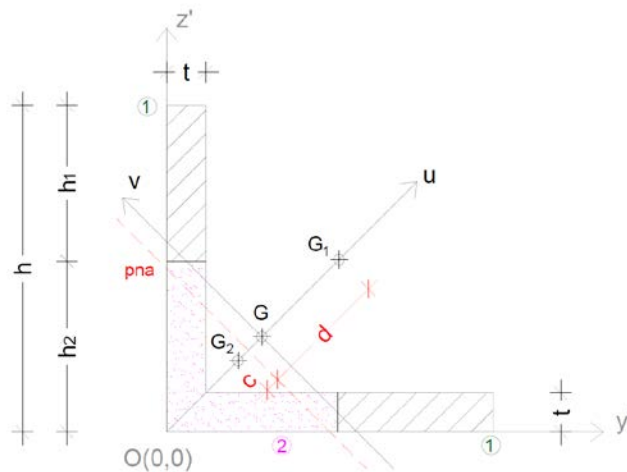$$y_{G_2} = \frac{h_2^2 + h_2 t - t^2}{4h_2 - 2t} \tag{2.16}$$

Figure 2.7: Notation for the calculation of the plastic modulus about v axis

From the numerical results, one can observe that the class-2 limit for equal leg angles subjected to weak axis bending is $c/t \leq 14\varepsilon$, while the class-3 limit it $c/t \leq 26{,}9\varepsilon$.

As explained in [2], the mechanical model for class 2 sections of Eurocode 3 when the tip is in compression is not correct, because the outstand elements partially in compression are treated as elements full in compression with a reduced width αc. For that reason, it is proposed here to keep the c/t limit for class 2 equal to:

$$\frac{c}{t} \leq 14\varepsilon \tag{2.17}$$

that is also in line with the numerical results.

The stress ratio for elastic stress distribution (see Figure 2.9) is given by $\psi = \frac{\sigma_2}{\sigma_1} = -\frac{e-(h-c)}{h-e} \approx -0{,}1$ for usual angle sections as it shown in [2]. Consequently, the buckling factor for clamped boundary conditions is equal to $k_\sigma = 1{,}65$ [9]. It should be noticed here that for class 3 limit, a clamped-free condition has been applied, as for strong axis bending. Then, the class-3 limit may be obtained from the general formula of EN 1993-1-1, Table 5.2, sheet 2:

$$\frac{c}{t} \leq 21\varepsilon\sqrt{K_\sigma} = 21\varepsilon\sqrt{1{,}65} = 26{,}9\varepsilon \tag{2.18}$$

The class-3 limit may be kept as calculated above, which is also on in agreement with the numerical results.

ANGELHY – Innovative solutions for design and strengthening of telecommunications and transmission lattice towers using large angles from high strength steel and hybrid techniques of angles with FRP strips
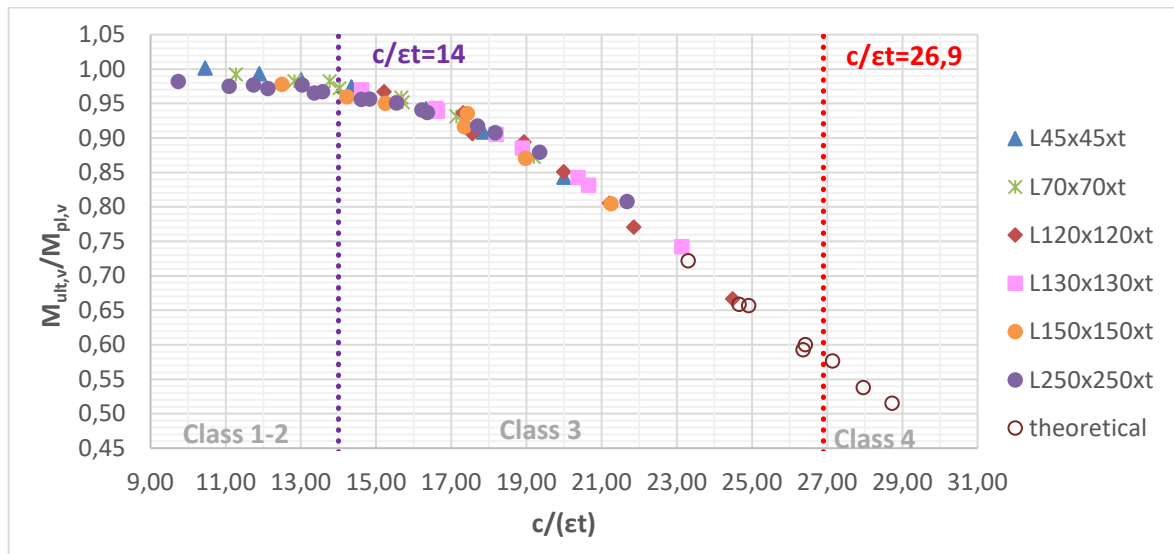
Page 14

Figure 2.8: Numerical results for the CS-resistance subjected to weak axis bending M$_v$ –tip in compression, related with the c/εt ratio
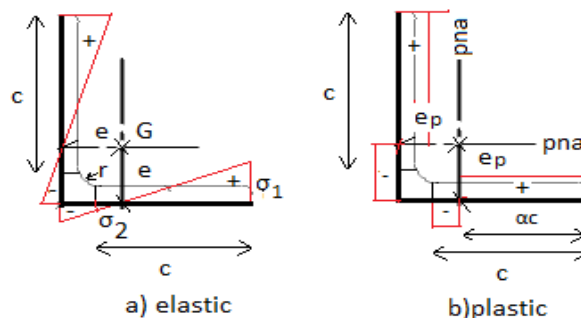

Figure 2.9: Stress distribution for weak axis bending (M$_v$) – tip in compression

2.5.2 Tip in tension

Table 2.6 presents the cross-sections and the steel grades that have been used for the analyses in which the pin-ended samples are subjected to weak axis bending moment M$_v$-tip in tension. As already explained for the previous cases, the last 8 analysis, i.e. 3* and 4* in Table 2.6 are theoretical so as to investigate the behaviour of the cross-section and validate the limit between class 2 and class 3.

Table 2.6: Details for the analyses of the cross-section subjected to weak axis bending M$_v$-tip in tension

No	Cross-Section	Steel grades
1	L120x120x7	S355 / S460 / S550 / S690
2	L120x120x8	S355 / S460 / S550 / S690
3*	L130x130x8	S720 / S850 / S1050 / S1250
4*	L130x130x9	S820 / S990 / S1200 / S2000

The value L=6h [mm] for the length has been adopted in this case too, as explained in 2.5.1. Figure 2.10 shows the ratio between the numerical results of for the cross-section resistance (M$_{ult,v}$) and the plastic characteristic resistance, versus the c/εt ratio, where c=h-t-r. The plastic resistance of the cross-section has been evaluated by using eq.(2.9).
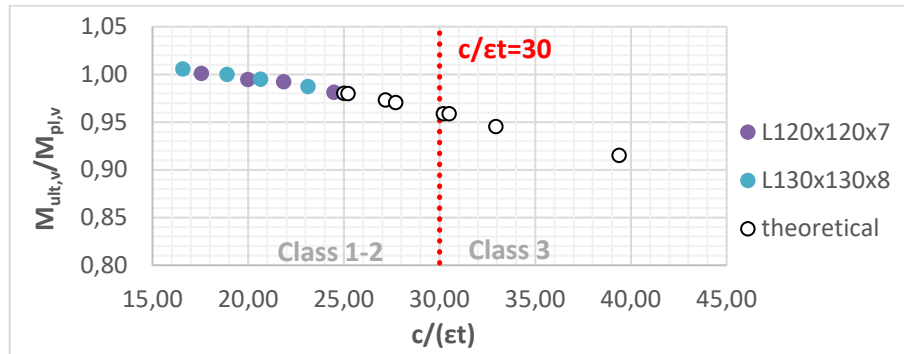
Figure 2.10: Numerical results for the CS-resistance subjected to weak axis bending M_v –tip in tension, related with the c/εt ratio

From the numerical results, one can observe that the class-2 limit for equal leg angles subjected to weak axis bending when the tip is in tension, equals $c/t \leq 30\varepsilon$.

The class-2 limit may be obtained from the general formula of EN 1993-1-1, Table 5.2, sheet 2:

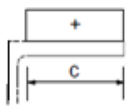$$\frac{c}{t} \leq \frac{10\varepsilon}{\alpha\sqrt{\alpha}} = \frac{10\varepsilon}{0,4\sqrt{0,4}} = 40\varepsilon \qquad (2.19)$$
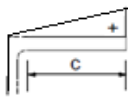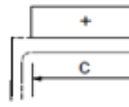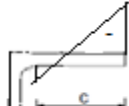
It has been shown in [2] that for usual angle sections it is a=0,4.
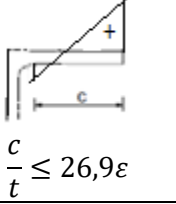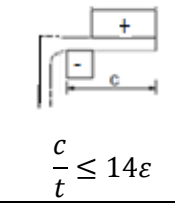
The class-2 limit may be kept as provided by the numerical results (c/t ≤ 30ε), which is on the safe side concerning the normative approach. In any case, both limits are far from the highest c/εt ratios obtained for available angles and steel grades. Therefore, all angle sections may practically always develop their plastic moment for weak axis bending when the tip is in tension.

2.6 Final proposal for the classification system

Table 2.7 summarizes the final proposal of the classification system for equal leg angle cross-sections. The proposed system has been validated through parametrical numerical simulations, always following the main principles of Eurocodes.

Table 2.7: Final proposal for the classification system for equal leg angle cross-sections

	Comment	Class 3	Class 2
Compression N_c			$\dfrac{c}{t} \leq 13,9\varepsilon$
Strong axis bending M_u		$\dfrac{c}{t} \leq 26,3\varepsilon$	$\dfrac{c}{t} \leq 16\varepsilon$
Weak axis bending M_v	Tip in tension		$\dfrac{c}{t} \leq 30\varepsilon$

Weak axis bending M_v	Tip in compression	$\frac{c}{t} \leq 26{,}9\varepsilon$	$\frac{c}{t} \leq 14\varepsilon$

3 Characteristic resistances of the cross-section

Based on the previous numerical simulations, a validation has been also done for the proposed formulae about the cross-section characteristic resistance for equal leg angles. In the following, the final proposal for the cross-section resistance is given, after has been validated by the numerical results.

3.1 Cross-section under pure compression

Two cases are distinguished in terms of the axial cross-section resistance: resistance of sections that are class 1,2 or 3 and resistance of the class 4 sections.

   i.   <u>Class 1, 2 and 3 cross-sections under pure compression</u>

The design resistance is equal to:

$$N_{c,Rk} = \frac{A f_y}{\gamma_{M0}}$$
(3.1)

where,

      A   is the area of the cross-section;

      f_y is the yielding stress of the material;

      γ_{M0} is material safety factor, equal to 1,0.

   ii.   <u>Class 4 cross-sections under pure compression</u>

The design resistance is equal to:

$$N_{c,Rk} = \frac{A_{eff} f_y}{\gamma_{M0}}$$
(3.2)

where,

      f_y is the yielding stress of the material;

      γ_{M0} is material safety factor, equal to 1,0;

      A_{eff} is the area of the effective cross-section that equals:

$$A_{eff} = A - 2ct(1 - \rho)$$
(3.3)

where:

      t   is the thickness of the legs;

      c   is equal to c=h-t-r;

      ρ is the reduction factor for plate buckling, calculating by the equations (3.4) and (3.5):

$$\rho = 1 \qquad\qquad \text{for } \bar{\lambda}_p \leq 0{,}748$$
(3.4)

$$\rho = \frac{\bar{\lambda}_p - 0{,}188}{\bar{\lambda}_p^2} \qquad\qquad \text{for } \bar{\lambda}_p > 0{,}748$$
(3.5)

      $\bar{\lambda}_p$ is the relative plate slenderness of legs:

$$\bar{\lambda}_p = \sqrt{\frac{\sigma_{com}}{\sigma_{cr}}} = \frac{c/t}{18{,}6\varepsilon}$$
(3.6)

For compatibility with the proposed classification limit for angles under pure compression as presented in the previous chapter, equation (3.14) from [2] should be replaced by equation (3.6) above. In addition, in EN 1993-1-5, §4.4(2) [11], where it is stated that $\bar{b} = h$ for equal leg angles should be replaced by "$\bar{b} = c$, for equal leg angles". Finally, equation (3.13) from [2] should be replaced by equation (3.3), which gives better results.

Figure 3.1 shows the ratio between the numerical results for the cross-section resistance (N_{ult}) and the analytical characteristic resistance, versus c/εt ratio. The analytical resistance of the cross-section has been evaluated by using the formulas presented in this section and both numerical and analytical results are in good agreement.
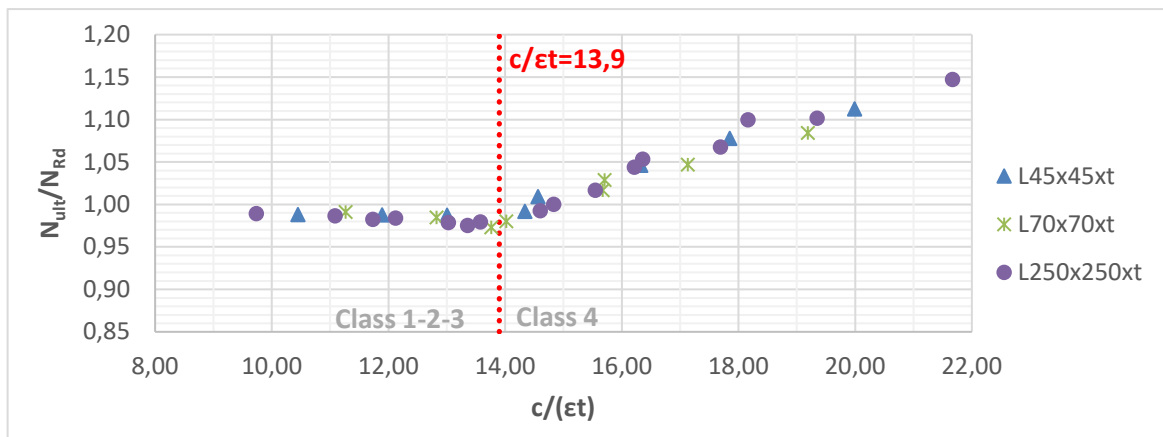
Figure 3.1: Comparison between numerical and analytical results for the CS-resistance subjected to a uniform axial load, related with the c/εt ratio

3.2 Cross-section subjected to strong axis bending

The design resistance of angle cross-sections subjected to strong axis bending is given by:

$$M_{u,Rk} = W_u \frac{f_y}{\gamma_{M0}} \tag{3.7}$$

where,

f_y is the yielding stress of the material;

γ_{M0} is material safety factor, equal to 1,0;

W_u is the parameter modulus about u axis that equals:

$$W_u = \alpha_{i,u} W_{el,u} \ , \ \ i = 2, 3, 4 \tag{3.8}$$

where,

$$\alpha_{2,u} = 1,5 \qquad\qquad\qquad \text{for class 1 or 2} \tag{3.9}$$

$$\alpha_{3,u} = \left[1 + \left(\frac{26,3\varepsilon - c/t}{26,3\varepsilon - 16\varepsilon}\right) \cdot (1,5 - 1)\right] \quad \text{for class 3} \tag{3.10}$$

$$\alpha_{4,u} = W_{eff,u} / W_{el,u} = \rho_u^2 \qquad\qquad \text{for class 4} \tag{3.11}$$

ρ_u is the reduction factor for plate buckling, calculating by the equations (3.12) and (3.13):

$$\rho_u = 1 \qquad\qquad \text{for } \bar{\lambda}_p \leq 0,748 \tag{3.12}$$

ANGELHY – Innovative solutions for design and strengthening of telecommunications and transmission lattice towers using large angles from high strength steel and hybrid techniques of angles with FRP strips

Page 18

$$\rho_u = \frac{\bar{\lambda}_p - 0,188}{\bar{\lambda}_p^2} \qquad \text{for } \bar{\lambda}_p > 0,748 \qquad (3.13)$$

$\bar{\lambda}_p$ is the relative plate slenderness of legs:

$$\bar{\lambda}_p = \sqrt{\frac{\sigma_{com}}{\sigma_{cr}}} = \frac{c/t}{35,58\varepsilon} \qquad (3.14)$$

The transition between the plastic and the elastic bending resistances follows the results of SEMICOMP [12] and so it is linear.

For strong axis bending, the effective cross-section becomes non-symmetric due to the fact that only one leg is in compression. This changes the position of the centroid, the directions of the principal axes and all cross-section properties. In order to avoid such laborious calculation, an approximate solution for the effective section modulus is envisaged. This may be achieved by reducing equally the other leg too. The comparison of the ratio between the two cross-sections is shown in Figure 3.2. It may be seen that the modulus of the effective cross section is approximately equal to the modulus of the initial cross-section multiplied with the square of the reduction factor, ρ_u^2 (for the cross-sections considered). The approach is theoretical (small value for thickness or high steel grade) as they do not exist so large $c/\varepsilon t$ ratios for hot-rolled equal leg angles.
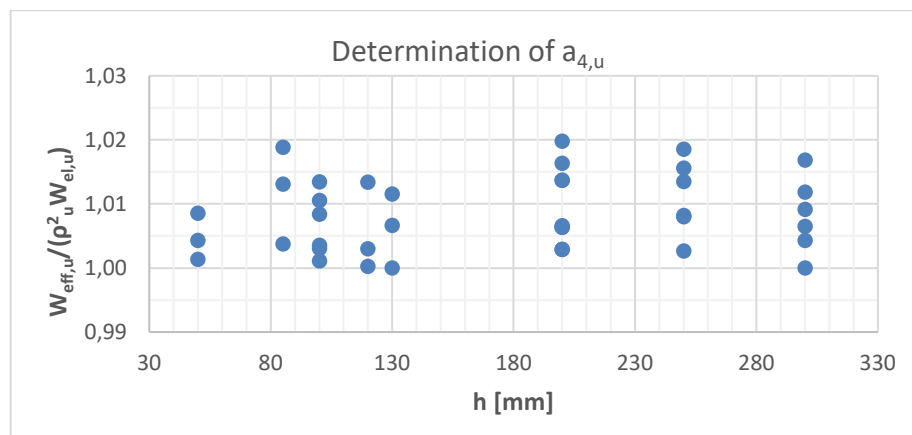
Figure 3.2: Ratio of the strong axis moduli between the initial and the effective cross-section

Figure 3.3 shows the ratio between the numerical results for the cross-section resistance ($M_{ult,u}$) and the analytical characteristic resistance, versus $c/\varepsilon t$ ratio. The analytical resistance of the cross-section has been calculated by using the formulas presented in this section. One could easily conclude that the analytical approach for the cross-section resistance subjected to strong axis bending is validated quite well by the numerical results.

ANGELHY – Innovative solutions for design and strengthening of telecommunications and transmission lattice towers using large angles from high strength steel and hybrid techniques of angles with FRP strips

Page 19

Figure 3.3: Comparison between numerical and analytical results for the CS-resistance subjected to strong axis bending moment M_u, related with the c/εt ratio

3.3 Cross-section subjected to weak axis bending

Two cases are defined and check afterwards in terms of cross-section resistance:

- the tip is in compression;
- the tip is in tension.

3.3.1 Tip in compression

The design resistance of angle cross-sections to weak axis bending M_v – tip in compression – is given by:

$$M_{v,Rk} = W_v \frac{f_y}{\gamma_{M0}} \tag{3.15}$$

where,

f_y is the yielding stress of the material;

γ_{M0} is material safety factor, equal to 1,0;

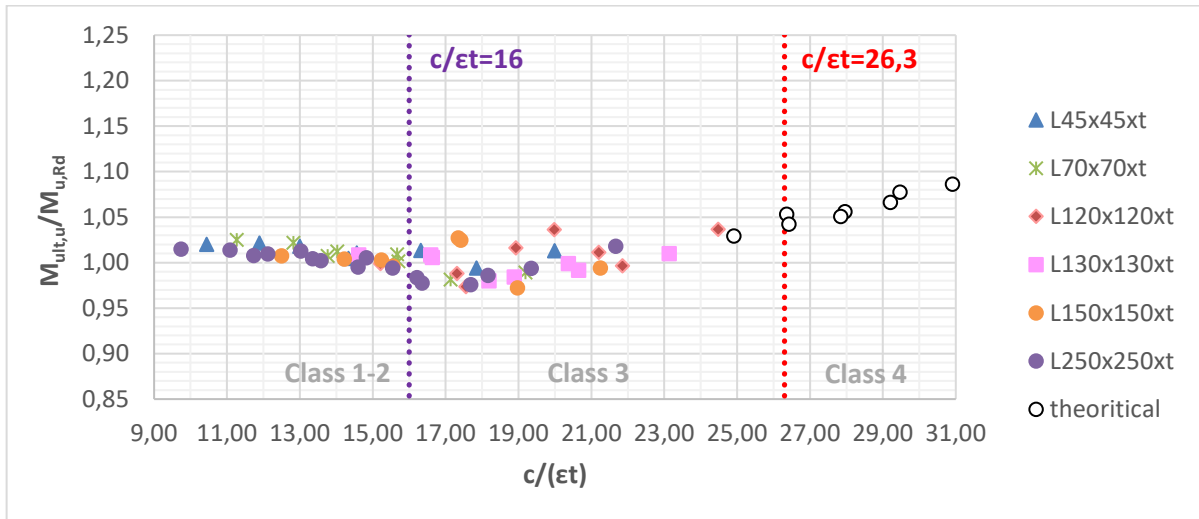W_v is the parameter modulus about v axis that equals:

$$W_v = \alpha_{i,v} W_{el,v} , \quad i = 2, 3, 4 \tag{3.16}$$

where,

$$\alpha_{2,v} = W_{pl,v} / W_{el,v} \qquad \text{for class 1 or 2} \tag{3.17}$$

$$\alpha_{3,v} = \left[1 + \left(\frac{26,9\varepsilon - c/t}{26,9\varepsilon - 14\varepsilon}\right) \cdot \left(\alpha_{2,v} - 1\right)\right] \qquad \text{for class 3} \tag{3.18}$$

$$\alpha_{4,v} = W_{eff,v} / W_{el,v} = 0,94 \cdot \rho_v^2 \qquad \text{for class 4} \tag{3.19}$$

ρ_v is the reduction factor for plate buckling, calculating by the equations (3.20) and (3.21):

$$\rho_v = 1 \qquad \text{for } \bar{\lambda}_p \leq 0,748 \tag{3.20}$$

$$\rho_v = \frac{\bar{\lambda}_p - 0,188}{\bar{\lambda}_p^2} \qquad \text{for } \bar{\lambda}_p > 0,748 \tag{3.21}$$

$\bar{\lambda}_p$ is the relative plate slenderness of legs:

ANGELHY – Innovative solutions for design and strengthening of telecommunications and transmission lattice towers using large angles from high strength steel and hybrid techniques of angles with FRP strips

Page 20

$$\bar{\lambda}_p = \sqrt{\frac{\sigma_{com}}{\sigma_{cr}}} = \frac{c/t}{36,48\varepsilon} \tag{3.22}$$

For the evaluation of the plastic modulus $W_{pl,v}$, equations (2.10) – (2.16) may be used. It should be noted that $W_{pl,v} \neq 1,50 \cdot \min(W_{el,v}^{tip}, W_{el,v}^{toe})$ in contrast with the case of strong axis bending. However, based on the numerical tested samples it is $W_{pl,v}=(1,65 \sim 1,95) \cdot \min(W_{el,v}^{tip}, W_{el,v}^{toe})$ and so, the value $\alpha_{2,v}=1,75$ could be possibly adopted.

The transition between elastic and plastic bending resistances adopts the results of SEMICOMP, also for weak axis bending.

For class 4 cross-sections a similar procedure as for strong axis bending is adopted. Figure 3.4 shows that the modulus of the effective cross section is approximately equal to the modulus of the initial cross-section multiplied with the factor, $0,94 \cdot \rho^2$. Therefore, $\alpha_{4,v}$ is fixed accordingly.
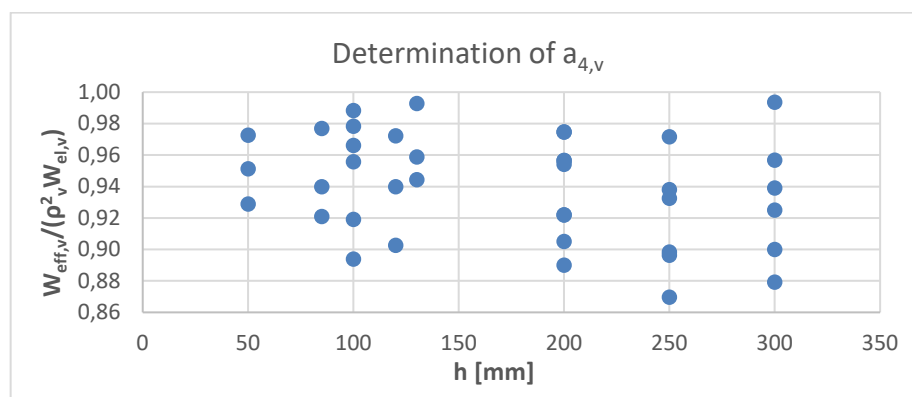
Figure 3.4: Ratio of the weak axis moduli between the initial and the effective cross-section

Figure 3.5 shows the ratio between the numerical results for the cross-section resistance ($M_{ult,v}$) and the analytical characteristic resistance, versus $c/\varepsilon t$ ratio. The analytical resistance of the cross-section has been calculated by using the formulas presented in this section. It can be seen that the analytical approach for the cross-section resistance subjected to weak axis bending with the tip is in compression, is validated quite well by the numerical results.

Figure 3.5: Comparison between numerical and analytical results for the CS-resistance subjected to weak axis bending moment M_v – tip in compression, related with the c/εt ratio

ANGELHY – Innovative solutions for design and strengthening of telecommunications   **Page 21**
and transmission lattice towers using large angles from high strength steel and hybrid
techniques of angles with FRP strips

3.3.2 Tip in tension

The design resistance of angle cross-sections to weak axis bending M_v – tip in tension – is given by:

$$M_{v,Rk} = W_{pl,v} \frac{f_y}{\gamma_{M0}} \qquad (3.23)$$

where,

  f_y is the yielding stress of the material;
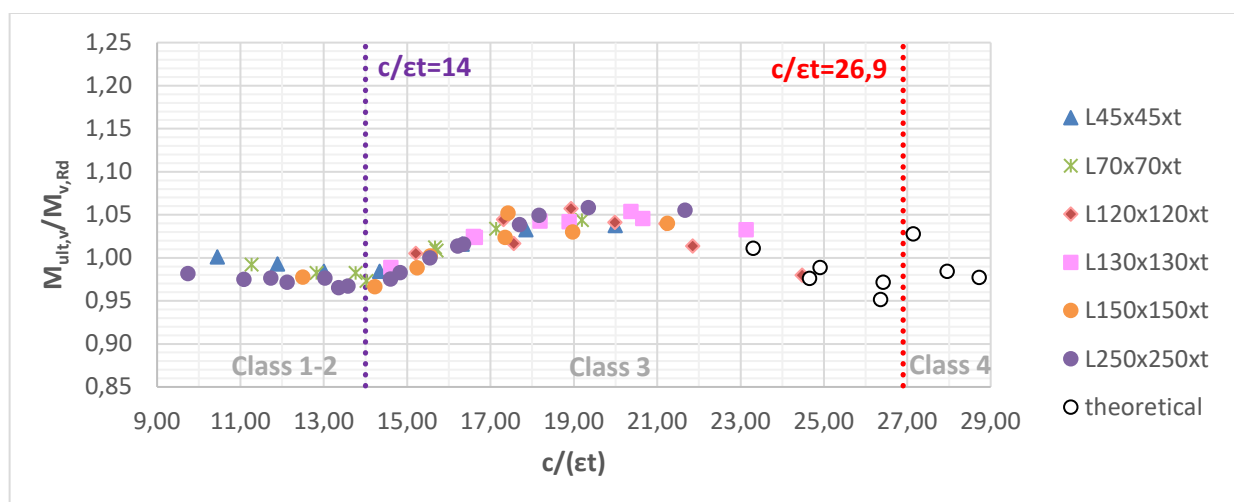
  γ_{M0} is material safety factor, equal to 1,0;

  $W_{pl,v}$ is the plastic modulus about v axis; eq. (2.10) – (2.16) may be used for the calculation.

As it is shown in Figure 2.10 for c/εt ratio less than 30, the analytical approach for the cross-section resistance subjected to weak axis bending when the tip is in tension is in good agreement with the numerical results.

4 Design formulae for the member resistance

The validation of the proposed formulae for the prediction of the carrying capacity of members with equal leg angle sections is based on comparisons with the results of numerical simulations of the member response of a wide range of specimens. As for the test samples, the profiles, the member lengths and the steel grades have been selected so as to reflect as much as possible members that are commonly used in pylons (see Table 4.1). In the following, only the final proposal for the member resistance is considered (not the intermediate versions). It should be also noticed here that the classification system used hereafter is the proposed one in chapter 2.

Table 4.1: Cross-sections that commonly used for pylons

Chords				Braces			
Cross-section	Use	Length [m]	Steel grades	Cross-section	Use	Length	Steel grades
L70x70xt	Smallest cross-section for upper levels	1,0-2,0	S355 S460	L80x80xt	For low levels	1,0-2,0	S355 S460
L150x150xt	Standard cross-section	2,0-3,0	S355 S460	L70x70xt	For middle levels	1,0-2,0	S355 S460
L250x250xt	For high pylons at low levels	2,0-3,0	S355 S460	L45x45xt	For upper levels	1,0-2,0	S355 S460

4.1 Numerical models

The numerical models for the validation of the member resistances were also performed with ABAQUS and were very similar with those that used for the validation of the classification system. The angle members were considered as pin-ended and have been modelled using at least three (3) volume elements per thickness as explained in 2.2, while fictitious end plates have been considered through a specific constraint at the extremities. A material law without strain hardening (see Figure 2.2), in accordance with EN 1993-1-14, has been used too.

The finite element analyses were performed considering:

* an initial bow imperfection of magnitude approximately equal to L[mm]/1000 with a deformation shape similar to the first member instability mode. This value is recommended be the European norm EN 1090-2 [13], which prescribes that the deviation from straightness

ANGELHY – Innovative solutions for design and strengthening of telecommunications and transmission lattice towers using large angles from high strength steel and hybrid techniques of angles with FRP strips

Page 22

should be $\Delta \leq L[mm]/750$ in combination with prEN 1993-1-14 [14] where it is stated that 80% of the geometric fabrication tolerances given in [13] should be applied.

- residual stresses resulting from the hot-rolling procedure. The selected pattern (Figure 4.1) is chosen from previous studies [15]-[16] in which appropriate measurements had been realized. It has to be taken into account that the residual stresses in hot rolled steel sections are independent of the steel grade and therefore a magnitude of $0{,}3 \cdot f_y$, that is approximately equal to 70 MPa for steel grade S235, is used.
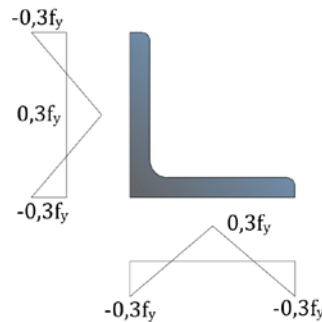

Figure 4.1: Assumed distribution pattern of residual stresses based on [15]-[16]

Due to some technical aspects of introducing residual stresses in the ABAQUS model, it has been decided to use an equivalent imperfection e_0 that will represent the effect of the combined action of both residual stresses and initial imperfections. To calibrate the value of the equivalent imperfection e_0, a few analyses have been performed with FINELG [17] finite element software, using beam elements. The angle members were considered as pin-ended with fictitious end plates at the extremities. The selection of the software has been done due to its easy and automatic way of introducing residual stresses in the model. The profiles and the material and geometrical properties of the tested samples are shown in Table 4.1.

First, a full-non linear analysis considering an initial imperfection (L/1000), an elastic perfectly plastic material law as well as residual stresses (using the pattern shown in Figure 4.1) has been performed for each one of the 10 different samples provided in Table 4.1 and the ultimate resistance N_{ult} has been recorded. By introducing this value (N_{ult}) to equation (4.1), a rough estimation of the equivalent imperfection e_0 can be found equal to $e_0 = L[mm]/700$ (initial calculated mean value L/757).

$$\sigma_{max} = \frac{N_{ult}}{A} + \frac{N_{ult}e_0}{\left(1 - \frac{N_{ult}}{N_{cr,v}}\right)W_v} = f_y \qquad (4.1)$$

Then a second full-non linear analysis, considering this time the equivalent imperfection (L/700) and an elastic perfectly plastic material law has been performed for each one of the 10 samples and the ultimate resistance N_{ult*} has been recorded and presented in Table 4.2. The mean value of the ratio N_{ult}/N_{ult*} is equal to 0,99 with a COV of 2,0%.

Table 4.2: Details and results from FINELG concerning the analyses to determine the equivalent imperfection e_0

No	Cross-Section	Length L [mm]	Steel grade	e_0 [mm] from eq. (4.1)	e_0=L/700 [mm]	N_{ult} [kN]	N_{ult*} [kN]	N_{ult}/N_{ult*} [-]
1	L70x70x5	1000	S355	1,34	1,42	182,41	188,45	0,97
2	L70x70x5	1000	S460	1,26	1,42	217,71	216,77	1,00
3	L70x70x5	2000	S355	2,69	2,86	64,04	64,77	0,99
4	L70x70x5	2000	S460	2,52	2,86	64,61	65,62	0,98
5	L80x80x8	2000	S355	2,74	2,86	144,31	142,03	1,02

ANGELHY – Innovative solutions for design and strengthening of telecommunications and transmission lattice towers using large angles from high strength steel and hybrid techniques of angles with FRP strips

Page 23

No	Cross-Section	Length L [mm]	Steel grade	e_0 [mm] from eq. (4.1)	$e_0=L/700$ [mm]	N_{ult} [kN]	N_{ult*} [kN]	N_{ult}/N_{ult*} [-]
6	L80x80x8	2000	S460	2,58	2,86	148,54	146,35	1,01
7	L150x150x13	2000	S355	2,89	2,86	1029,72	1077,83	0,96
8	L150x150x13	2000	S460	2,73	2,86	1259,42	1267,67	0,99
9	L250x250x20	2000	S355	2,87	2,86	3156,6	3236,49	0,98
10	L250x250x20	2000	S460	2,67	2,86	4005,27	3939,71	1,02

Finally, a third full-non linear analysis, considering the equivalent imperfection (L/700) has been performed with ABAQUS using solid elements. The mean value of the ratio $N_{ult,abaqus}/N_{ult}$ is equal to 0,96 with a COV of 3,3%, which can be acceptable considering the different types of finite elements used in the two models (beam elements in FINELG and solid element in ABAQUS). Therefore, the equivalent imperfection $e_0=L[mm]/700$ is finally used at the analyses performed with ABAQUS to validate the member resistances.

4.2 Member under pure compression

Two cases are distinguished in terms of the axial cross-section resistance: sections that are class 1,2 or 3 and the class 4 sections.

i. Class 1, 2 and 3 cross-sections under pure compression

The proposed design resistance is equal to:

$$N_{b,Rd} = \frac{\chi_{min} A f_y}{\gamma_{M1}} \qquad (4.2)$$

where,

χ_{min} is the buckling reduction factor which should be determined as a function of the relative slenderness $\bar{\lambda}$ of the compression member, see 4.2.1;

A   is the area of the cross-section;

f_y is the yielding stress of the material;

γ_{M1} is the safety factor for buckling, equal to 1,0.

ii. Class 4 cross-sections under pure compression

The proposed design resistance is equal to:

$$N_{b,Rd} = \frac{\chi_{min} A_{eff} f_y}{\gamma_{M1}} \qquad (4.3)$$

where,

χ_{min} is the buckling reduction factor which should be determined as a function of the relative slenderness $\bar{\lambda}$ of the compression member, see 4.2.1;

f_y is the yielding stress of the material;

γ_{M1} is the safety factor for buckling, equal to 1,0.

A_{eff} is the area of the effective cross-section that equals:

$$A_{eff} = A - 2ct(1-\rho) \qquad (4.4)$$

where:

t   is the thickness of the legs;

c   is equal to c=h-t-r;

ρ is the reduction factor for plate buckling, calculating by the equations (4.5) and (4.6):

$$\rho = 1 \qquad\qquad \text{for } \bar{\lambda}_p \leq 0,748 \qquad\qquad (4.5)$$

$$\rho = \frac{\bar{\lambda}_p - 0,188}{\bar{\lambda}_p^2} \qquad \text{for } \bar{\lambda}_p > 0,748 \qquad\qquad (4.6)$$

$\bar{\lambda}_p$ is the relative plate slenderness of legs:

$$\bar{\lambda}_p = \sqrt{\frac{\sigma_{com}}{\sigma_{cr}}} = \sqrt{\chi_{min}}\frac{c/t}{18,6\varepsilon} \qquad\qquad (4.7)$$

4.2.1 Determination of χ_min

The buckling reduction factor should be determined as a function of the relative slenderness $\bar{\lambda}$ of the compression member for the flexural buckling modes only:

$$\chi_{min} = \{\chi_u; \chi_v\} \qquad\qquad (4.8)$$

The relative slenderness $\bar{\lambda}$ should be taken as:

$$\bar{\lambda} = \sqrt{\frac{Af_y}{N_{cr}}} \qquad\qquad (4.9)$$

where,

        A   is the area of the cross-section;

        f_y is the yielding stress of the material;

        N_{cr} is the minimum elastic critical force for the flexural buckling mode based on the gross cross-sectional properties, i.e $N_{cr}=\min\{N_{cr,u};N_{cr,v}\}$

        $N_{cr,u}$ for elastic flexural buckling about u-u, leading to $\overline{\lambda_u}$;

        $N_{cr,v}$ for elastic flexural buckling about v-v, leading to $\overline{\lambda_v}$;

The value of the buckling reduction factor χ for the appropriate relative slenderness $\bar{\lambda}$ should be determined from the relevant buckling curve according to the equations (8.73)-(8.74) in combination with tables 8.2 and 8.3 of prEN 1993-1-1: §8.3.1.3[1], i.e curve b is used for steel grades S235-S420 while curve a is used for steel higher grades (≥S460).

4.2.2 Numerical validation

The profiles, lengths and steel grades have been selected from Table 4.1, but the thicknesses have been chosen so as to have samples of different classes (class 1 and 4) but also different buckling modes as flexural or flexural-torsional. A pure torsional mode cannot be obtained for a centrally loaded angle column as explained in [18]. The details are summarized in Table 4.3, including also the ratio of the elastic critical load for flexural-torsional buckling by the minimum one obtained for flexural buckling.

Table 4.3: Details for the samples subjected to a uniform compression load

No	Cross-Section	L [mm]	f_y [N/mm²]	c/(εt)	Class	Eigenmode deformed shape	$N_{cr,FT}/\min N_{cr,F}$ [-]
1		1000	355	13,77	1	Flexural	1,05
2	L70x70x5	1000	460	15,67	4	Flexural	1,05
3		2000	355	13,77	1	Flexural	2,64
4		2000	460	15,67	4	Flexural	2,64
5		1000	355	11,27	1	Flexural	1,43
6	L70x70x6	1000	460	12,82	1	Flexural	1,43
7		2000	355	11,27	1	Flexural	3,01
8		2000	460	12,82	1	Flexural	3,01

ANGELHY – Innovative solutions for design and strengthening of telecommunications   **Page 25**
and transmission lattice towers using large angles from high strength steel and hybrid
techniques of angles with FRP strips

No	Cross-Section	L [mm]	f_y [N/mm²]	$c/(\varepsilon t)$	Class	Eigenmode deformed shape	$N_{cr,FT}/minN_{cr,F}$ [-]
9		1000	355	9,48	1	Flexural	1,82
10	L70x70x7	1000	460	10,79	1	Flexural	1,82
11		2000	355	9,48	1	Flexural	3,25
12		2000	460	10,79	1	Flexural	3,25
13		1000	355	6,27	1	Flexural	2,71
14	L70x70x10	1000	460	7,14	1	Flexural	2,71
15		2000	355	6,27	1	Flexural	3,53
16		2000	460	7,14	1	Flexural	3,53
17		2000	355	11,44	1	Flexural	1,29
18	L150x150x13	2000	460	13,02	1	Flexural	1,29
19		3000	355	11,44	1	Flexural	2,25
20		3000	460	13,02	1	Flexural	2,25
21		2000	355	10,53	1	Flexural	1,46
22	L150x150x14	2000	460	11,99	1	Flexural	1,46
23		3000	355	10,53	1	Flexural	2,44
24		3000	460	11,99	1	Flexural	2,44
25		2000	355	9,75	1	Flexural	1,63
26	L150x150x15	2000	460	11,10	1	Flexural	1,63
27		3000	355	9,75	1	Flexural	2,61
28		3000	460	11,10	1	Flexural	2,61
29		2000	355	7,92	1	Flexural	2,11
30	L150x150x18	2000	460	9,02	1	Flexural	2,11
31		3000	355	7,92	1	Flexural	2,98
32		3000	460	9,02	1	Flexural	2,98
33		2000	355	15,54	4	Flexural-torsional	0,32
34	L250x250x17	2000	460	17,69	4	Flexural-torsional	0,32
35		3000	355	15,54	4	Flexural-torsional	0,69
36		3000	460	17,69	4	Flexural-torsional	0,69
37		2000	355	13,03	1	Flexural-torsional	0,45
38	L250x250x20	2000	460	14,83	4	Flexural-torsional	0,45
39		3000	355	13,03	1	Flexural-torsional	0,99
40		3000	460	14,83	4	Flexural-torsional	0,99
41		2000	355	11,73	1	Flexural-torsional	0,54
42	L250x250x22	2000	460	13,35	1	Flexural-torsional	0,54
43		3000	355	11,73	1	Flexural	1,11
44		3000	460	13,35	1	Flexural	1,11
45		2000	355	9,74	1	Flexural-torsional	0,75
46	L250x250x26	2000	460	11,09	1	Flexural-torsional	0,75
47		3000	355	9,74	1	Flexural	1,48
48		3000	460	11,09	1	Flexural	1,48

The samples have been modelled as explained in §4.1. However, for those where the first elastic eigenmode is a flexural-torsional one, three cases were considered in terms of initial imperfections:

    a. equivalent imperfection e_0 with a deformation shape similar to the first member instability mode, i.e. the flexural-torsional one (which correspond to $N_{ult(a)}$);

b. equivalent imperfection e_0 with a deformation shape similar to the first flexural instability mode (which correspond to $N_{ult(b)}$);

c. equivalent imperfection e_0 with a deformation shape similar to the first member instability mode (flexural-torsional) and equivalent imperfection e_0 with a deformation shape similar to the first flexural instability mode (which correspond to $N_{ult(c)}$);

The difference between the values $N_{ult(b)}$ and $N_{ult(c)}$ is negligible (less than 0,5%) but in the latter there is also a twist of the cross-section.

Figure 4.2 illustrates the numerical results compared with the reference buckling curves a and b. The buckling reduction factor χ_{num} of the tested samples has been evaluated by the equation $\chi_{num}=N_{num}/N_{pl}$ and the slenderness using eq.(4.9). For the samples with a flexural-torsional eigenmode, two cases are distinguished in Figure 4.2. The numerical results reported with blue/orange points have been evaluated using $N_{ult}=\min\{N_{ult(a)}, N_{ult(b)}, N_{ult(c)}\}$, while the results presented with green points using $N_{ult}=N_{ult(a)}$.
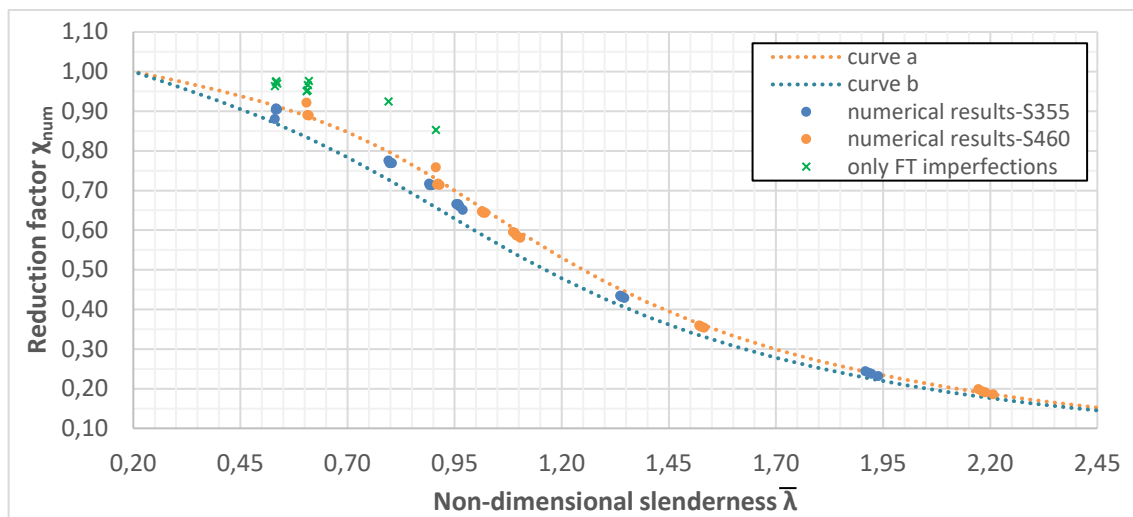
Figure 4.2: Comparison of numerical results with buckling curves of EN 1993-1-1
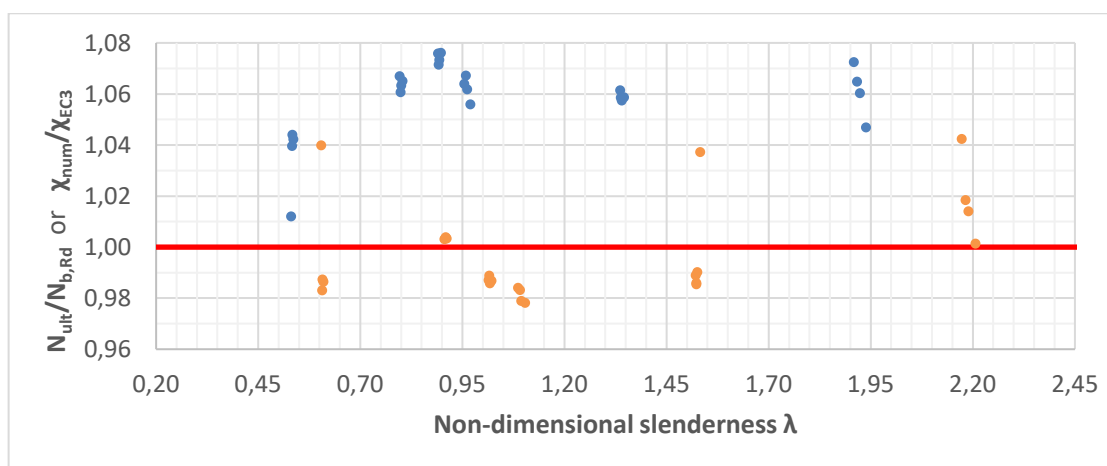

Figure 4.3: Comparison between numerical and analytical results for the resistance of members subjected to a uniform axial load, related with the non-dimensional slenderness

According to [1], the obtained numerical results for the S355 steel grade should be compared with curve b while for S460 with curve a. It can be easily observed that all the results referred to curve b

ANGELHY – Innovative solutions for design and strengthening of telecommunications   **Page 27**
and transmission lattice towers using large angles from high strength steel and hybrid
techniques of angles with FRP strips

are above the curve, while the results referred to curve a are in line, above or just a bit lower, which is acceptable given the 2% deviation that is considered. Regarding the results obtained using only an equivalent imperfection based on the 1st eigenmode (i.e. the flexural-torsional one), it is obvious that are much higher even they compared with curve a. Through this comparison, it can be easily observed that the slenderness should be calculated using only the minimum elastic critical force for the flexural buckling mode.

Figure 4.3 shows the ratio between the numerical results for the member resistance (N_{ult}) and the analytical resistance ($N_{b,Rd}$), versus the non-dimensional slenderness. The analytical resistance has been evaluated by using the formulas presented in this section and validated through the numerical results as both are in good agreement and a 2% deviation is acceptable.

4.3 Member subjected to strong axis bending

The proposed design resistance of angle cross-sections to strong axis bending considering the effects of lateral torsional buckling (LTB) is given by:

$$M_{u,Rd} = \chi_{LT} W_u \frac{f_y}{\gamma_{M1}} \tag{4.10}$$

where,

χ_{LT} is the buckling reduction factor which should be determined as a function of the relative slenderness $\overline{\lambda_{LT}}$ of the compression member, see 4.3.1;

f_y is the yielding stress of the material;

γ_{M1} is the safety factor for buckling, equal to 1,0.

W_u is the parameter modulus about u axis that equals:

$$W_u = \alpha_{i,u} W_{el,u} , \quad i = 2, 3, 4 \tag{4.11}$$

where,

$$\alpha_{2,u} = 1,5 \qquad\qquad\qquad \text{for class 1 or 2} \tag{4.12}$$

$$\alpha_{3,u} = \left[1 + \left(\frac{26,3\varepsilon - c/t}{26,3\varepsilon - 16\varepsilon}\right) \cdot (1,5 - 1)\right] \quad \text{for class 3} \tag{4.13}$$

$$\alpha_{4,u} = W_{eff,u}/W_{el,u} = \rho_u^2 \qquad\qquad \text{for class 4} \tag{4.14}$$

ρ_u is the reduction factor for plate buckling, calculating by the equations (4.15) and (4.16):

$$\rho_u = 1 \qquad\qquad\qquad \text{for } \bar{\lambda}_p \leq 0,748 \tag{4.15}$$

$$\rho_u = \frac{\bar{\lambda}_p - 0,188}{\bar{\lambda}_p^2} \qquad\qquad \text{for } \bar{\lambda}_p > 0,748 \tag{4.16}$$

$\bar{\lambda}_p$ is the relative plate slenderness of legs:

$$\bar{\lambda}_p = \sqrt{\frac{\sigma_{com}}{\sigma_{cr}}} = \sqrt{\chi_{LT}} \frac{c/t}{35,58\varepsilon} \tag{4.17}$$

4.3.1 Determination of χ_{LT}

The reduction factor for lateral torsional buckling χ_{LT} should be determined as a function of the relative slenderness $\overline{\lambda_{LT}}$ of the member:

$$\overline{\lambda_{LT}} = \sqrt{\frac{W_u f_y}{M_{cr}}} \tag{4.18}$$

ANGELHY – Innovative solutions for design and strengthening of telecommunications and transmission lattice towers using large angles from high strength steel and hybrid techniques of angles with FRP strips

Page 28

where,

Wu   is the parameter modulus about u axis that equals, see equations (4.11)-(4.14);

f_y is the yielding stress of the material;

M_{cr} is the elastic critical moment for lateral-torsional buckling, given by equation (4.19) with use of Table 4.4:

$$M_{cr} = C_b \frac{0,46 \cdot E \cdot h^2 \cdot t^2}{l} \qquad (4.19)$$

Table 4.4: Determination of the C_b-factor for LTB

<u>**General case:**</u>

$$C_b = \frac{12,5 M_{max}}{2,5 M_{max} + 3 M_A + 4 M_B + 3 M_C} \leq 1,5$$

<u>**For linear moment distribution:**</u>

$$C_b = \frac{12,5}{7,5 + 5\psi} \quad \text{with} \quad -1 \leq \psi = \frac{M_2}{M_1} \leq 1$$

The value of the buckling reduction factor χ_{LT} for the relative slenderness $\overline{\lambda_{LT}}$ should be derived from buckling curve **a**. The buckling curve can be determined by the equation (6.57) of EN 1993-1-1: §6.3.2.3(1) for lateral-torsional buckling [19], using $\bar{\lambda}_{LT,0} = 0,4$ and β=1,00 (see eq.(4.20) below).

$$\chi_{LT} = \frac{1}{\Phi_{LT} + \sqrt{\Phi_{LT}^2 - \bar{\lambda}_{LT}^2}} \quad \text{but} \quad \begin{cases} \chi_{LT} \leq 1,0 \\ \chi_{LT} \leq 1/\bar{\lambda}_{LT}^2 \end{cases} \qquad (4.20a)$$

$$\Phi_{LT} = 0,5\left[1 + a_{LT}(\bar{\lambda}_{LT} - 0,4) + \bar{\lambda}_{LT}^2\right] \qquad (4.20b)$$

Lateral torsional buckling may be ignored and χ_{LT} set equal to 1,0 when one of the following conditions apply:

- $\bar{\lambda}_{LT} \leq \bar{\lambda}_{LT,0}$ with $\bar{\lambda}_{LT,0} = 0,4$

- $\frac{M_{Ed}}{M_{cr}} \leq \bar{\lambda}_{LT,0}^{\,2}$

- $\frac{N_{Ed}}{N_{bu,Rd}} > 0,5$

- $\frac{N_{Ed}}{N_{bv,Rd}} > 0,5$

4.3.2 Numerical validation

For this load case, the profiles, lengths and steel grades have been again selected from Table 4.1, while the thicknesses have been chosen to have samples of different classes (1 and 3). It has already been explained that there are no hot-rolled angle profiles with steel grades (S355 or S460) that are categorized as class 4. The details are summarized in Table 4.5. To extend the field of investigation, 8 analyses have been additionally considered (marked with * in the mentioned table) with higher steel grades and member lengths so as to study some more slender members. For each non-linear analysis, an initial imperfection of magnitude L[mm]/700 has been applied with a deformation shape similar to the first member instability mode to introduce a twist imperfection at the middle cross-section (see

ANGELHY – Innovative solutions for design and strengthening of telecommunications **Page 29**
and transmission lattice towers using large angles from high strength steel and hybrid
techniques of angles with FRP strips

Figure 4.4). It should be also noticed that the mean value of the ratio $M_{cr,num}/M_{cr,anal}$ is equal to 0,989 with a COV of 4%.

Table 4.5: Details for the samples subjected to a major axis bending moment

No	Cross-Section	L [mm]	f_y [N/mm²]	Class	No	Cross-Section	L [mm]	f_y [N/mm²]	Class
1		1000	355	1	29		2000	355	1
2	L 45x45x3	1000	460	3	30	L 250x250x17	2000	460	3
3		2000	355	1	31		3000	355	1
4		2000	460	3	32		3000	460	3
5		1000	355	1	33		2000	355	1
6	L70x70x5	1000	460	1	34	L 250x250x20	2000	460	1
7		2000	355	1	35		3000	355	1
8		2000	460	1	36		3000	460	1
9		1000	355	1	37		2000	355	1
10	L70x70x6	1000	460	1	38	L 250x250x22	2000	460	1
11		2000	355	1	39		3000	355	1
12		2000	460	1	40		3000	460	1
13		2000	355	1	41		4000	355	1
14	L 80x80x5	2000	460	3	42	L 250x250x22*	4000	460	1
15		3000	355	1	43		5000	355	1
16		3000	460	3	44		5000	460	1
17		2000	355	1	45		4000	550	1
18	L150x150x13	2000	460	1	46	L 250x250x22*	4000	690	3
19		3000	355	1	47		5000	55	1
20		3000	460	1	48		5000	690	3
21		2000	355	1	49		2000	355	1
22	L150x150x14	2000	460	1	50	L 250x250x26	2000	460	1
23		3000	355	1	51		3000	355	1
24		3000	460	1	52		3000	460	1
25		2000	355	1					
26	L150x150x15	2000	460	1					
27		3000	355	1					
28		3000	460	1					
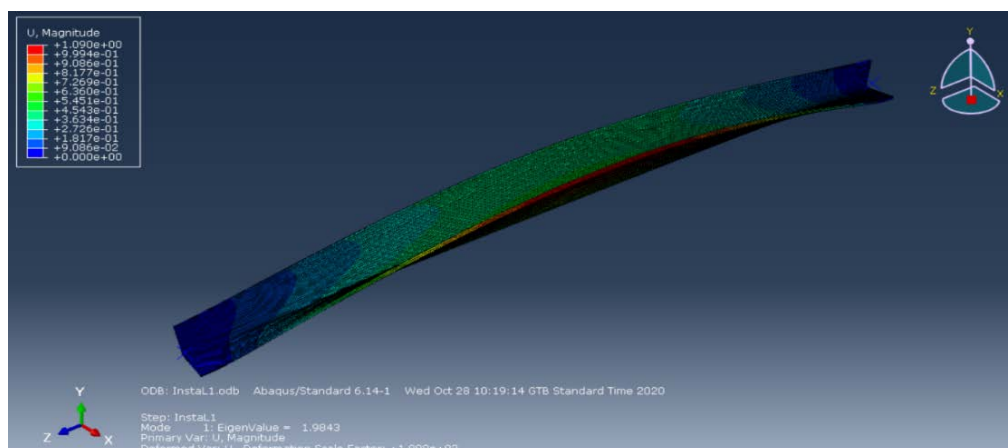
Figure 4.4: Typical shape of initial imperfections for a member subjected to strong axis bending

Figure 4.5 illustrates the numerical results compared with the buckling curves a and a_0 for LTB as they defined by eq. (4.20). The reduction factor for lateral torsional buckling $\chi_{LT,num}$ of the tested samples has been evaluated by the equation $\chi_{LT,num}=M_{num,u}/W_u f_y$ (see eq.(4.11) for the determination of W_u) and the slenderness by using eq.(4.18).
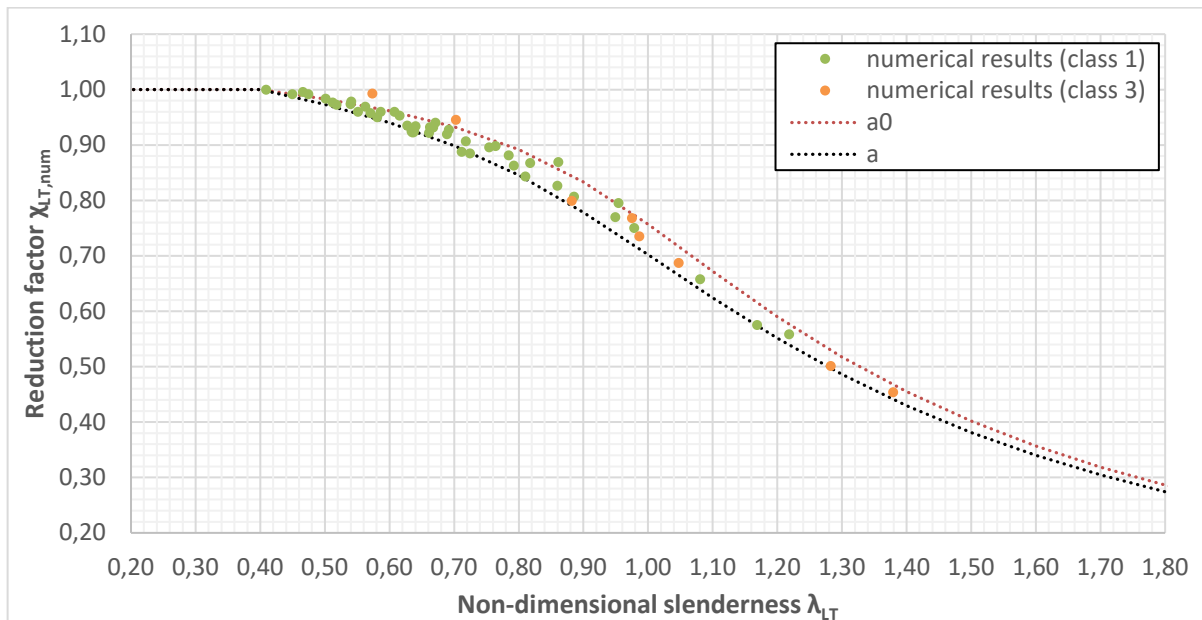

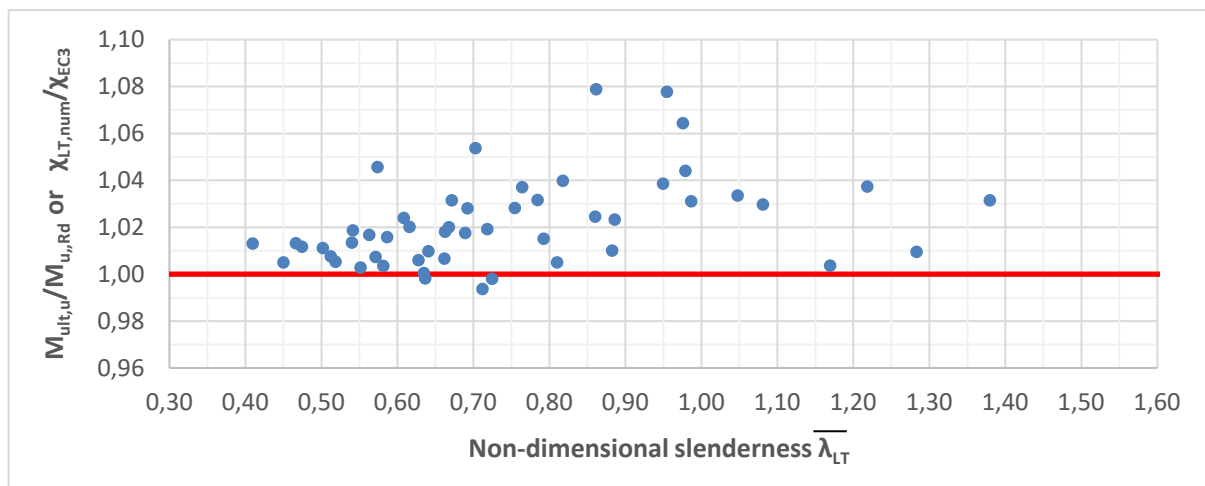**Figure 4.5: Comparison of numerical results with buckling curves for LTB of EN 1993-1-1**

Figure 4.6: Comparison between numerical and analytical results for the resistance of members subjected to strong axis bending, related with the non-dimensional slenderness

It is clear through the graph that all the results are above curve a and below curve a_0, and this validates the proposed buckling curve for LTB of angle sections. However, it seems that the resistance of some class-3 profiles is above curve a_0. This could be explained by the fact that these cross-sections are classified as class 3 but with a $c/\varepsilon t$ ratio quite close to the class-2 limit, and so they are treated as class 3 sections while in reality, they reach their plastic resistance. On the contrary, due to the integration of the SEMI-COMP aspects, a profile classified as Class 3, but very close to Class 2, should be characterized by a section resistance close to M_{pl}. To set this clear, one should have in mind the small scatter in Figure 2.5, where it can be seen that a profile with a $c/\varepsilon t$ approximately equal to 16, could

ANGELHY – Innovative solutions for design and strengthening of telecommunications **Page 31**
and transmission lattice towers using large angles from high strength steel and hybrid
techniques of angles with FRP strips

have a ratio $M_{ult,u}/M_{pl}$ from 0,95 to 1,0. This justifies the increased value of the numerical results. It should be also noticed that for higher $c/\varepsilon t$ ratios, the results conform better to curve a.

Figure 4.6 shows the ratio between the numerical member resistance ($M_{ult,u}$) and the analytical resistance ($M_{u,Rd}$), versus the non-dimensional slenderness. The analytical resistance has been evaluated by using the formulas presented in this section and validated through the numerical results.

4.4 Member subjected to weak axis bending

4.4.1 Tip in compression

The proposed design resistance of angle cross-sections to weak axis bending M_v – tip in compression – is given by:

$$M_{v,Rd} = W_v \frac{f_y}{\gamma_{M0}} \tag{4.21}$$

where,

f_y is the yielding stress of the material;

γ_{M0} is the material safety factor, equal to 1,0.

W_v is the parameter modulus about v axis that equals:

$$W_v = \alpha_{i,v} W_{el,v} , \quad i = 2, 3, 4 \tag{4.22}$$

where,

$$\alpha_{2,v} = W_{pl,v}/W_{el,v} \qquad \text{for class 1 or 2} \tag{4.23}$$

$$\alpha_{3,v} = \left[1 + \left(\frac{26,9\varepsilon - c/t}{26,9\varepsilon - 14\varepsilon}\right) \cdot \left(\alpha_{2,v} - 1\right)\right] \qquad \text{for class 3} \tag{4.24}$$

$$\alpha_{4,v} = W_{eff,v}/W_{el,v} = 0,94 \cdot \rho_v^2 \qquad \text{for class 4} \tag{4.25}$$

ρ_v is the reduction factor for plate buckling, calculating by the equations (4.26) and (4.27):

$$\rho_v = 1 \qquad\qquad \text{for } \bar{\lambda}_p \leq 0,748 \tag{4.26}$$

$$\rho_v = \frac{\bar{\lambda}_p - 0,188}{\bar{\lambda}_p^2} \qquad \text{for } \bar{\lambda}_p > 0,748 \tag{4.27}$$

$\bar{\lambda}_p$ is the relative plate slenderness of legs:

$$\bar{\lambda}_p = \sqrt{\frac{\sigma_{com}}{\sigma_{cr}}} = \frac{c/t}{36,48\varepsilon} \tag{4.28}$$

For the evaluation of the plastic modulus $W_{pl,v}$, equations (2.10) – (2.16) may be used.

4.4.2 Tip in tension

The proposed design resistance of angle cross-sections to weak axis bending M_v – tip in tension – is given by:

$$M_{v,Rd} = W_{pl,v} \frac{f_y}{\gamma_{M0}} \tag{4.29}$$

where,

f_y is the yielding stress of the material;

γ_{M0} is material safety factor, equal to 1,0;

$W_{pl,v}$ is the plastic modulus about v axis; eq. (2.10) – (2.16) may be used for the calculation.

4.4.3 Numerical validation

The design resistance of angle cross-sections to weak axis bending M_v, ether the tip is in tension or compression, is independent of the member's length. Therefore, just a few analyses have been performed to validate the proposed formulas additionally with the analyses presented in §2.5. Again, the profiles, lengths and steel grades have been chosen from Table 4.1, and the details are summarized in Table 4.6.

Table 4.6: Details for the samples subjected to a weak axis bending moment

	Tip in compression					Tip in tension			
No	Cross-Section	L [mm]	f_y [N/mm²]	Class	No	Cross-Section	L [mm]	f_y [N/mm²]	Class
1		1000	355	1	1		1000	355	1
2	L70x70x5	1000	460	3	2	L45x45x3	1000	460	1
3		2000	355	1	3		2000	355	1
4		2000	460	3	4		2000	460	1
5		2000	355	1	5		1000	355	1
6	L150x150x14	2000	460	1	6	L70x70x6	1000	460	1
7		3000	355	1	7		2000	355	1
8		3000	460	1	8		2000	460	1
9		2000	355	3	9		2000	355	1
10	L250x250x17	2000	460	3	10	L250x250x20	2000	460	1
11		3000	355	3	11		3000	355	1
12		3000	460	3	12		3000	460	1

Figure 4.7 and Figure 4.8 shows the ratio between the numerical results for the member resistance ($M_{ult,v}$) and the analytical resistance ($M_{v,Rd}$) when the tip is in compression and in tension respectively. It can be seen that the analytical approach for the resistance of a member subjected to weak axis bending, is validated quite well through the numerical results by accepting a 2% deviation.
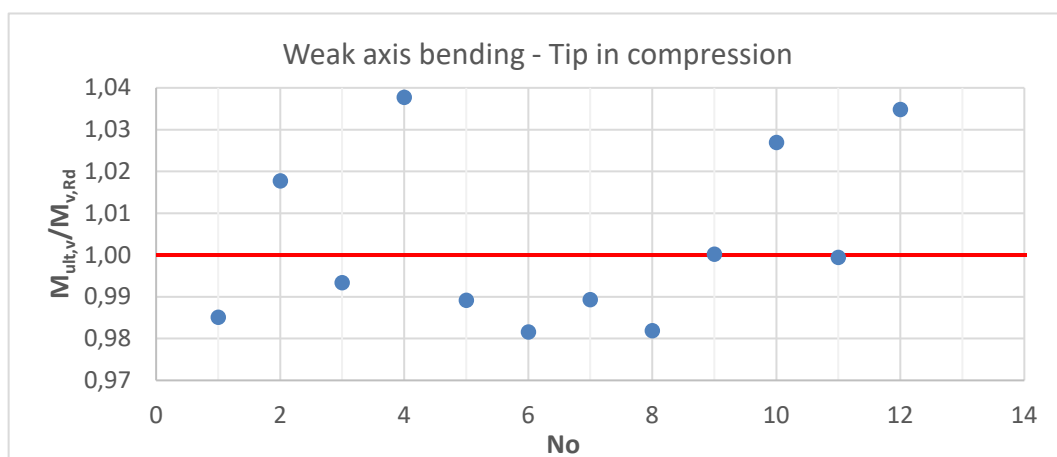
Figure 4.7: Comparison between numerical and analytical results for the resistance of members subjected to weak axis bending with the tip in compression
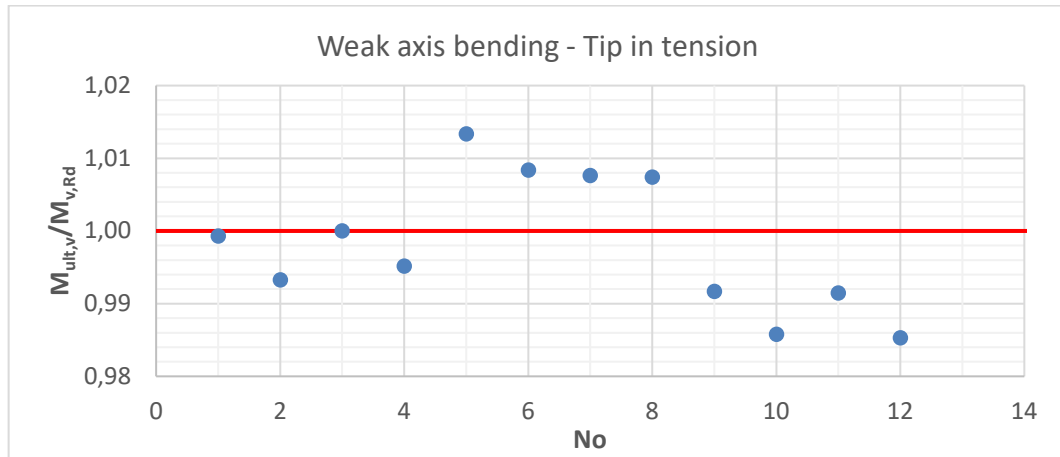
Figure 4.8: Comparison between numerical and analytical results for the resistance of members subjected to weak axis bending with the tip in tension.

4.5 Member subjected to bending and axial compression

For angle members subjected to compression and bending, two checks for buckling around one or the other principal axis should be satisfied according to this proposal. The lateral torsional buckling is included in the strong axis bending term while local buckling is taken into account through the properties of the effective section.

- strong axis check

$$\left(\frac{N_{Ed}}{N_{bu,Rd}} + k_{uu}\frac{M_{u,Ed}}{M_{u,Rd}}\right)^{\xi} + k_{uv}\frac{M_{v,Ed}}{M_{v,Rd}} \leq 1 \tag{4.30}$$

- weak axis check

$$\left(\frac{N_{Ed}}{N_{bv,Rd}} + k_{vu}\frac{M_{u,Ed}}{M_{u,Rd}}\right)^{\xi} + k_{vv}\frac{M_{v,Ed}}{M_{v,Rd}} \leq 1 \tag{4.31}$$

where,

N_{Ed} is the axial force;

$N_{bu,Rd}$ is the design value of the buckling resistance of a member in compression about u-u axis (see §4.2);

$N_{bv,Rd}$ is the design value of the buckling resistance of a member in compression about v-v axis (see §4.2);

$M_{u,Ed}$ is the bending moment about u axis ($M_{u,Ed}=N_{Ed}(e_v+e_{initial})$);

$M_{u,Rd}$ is the design value of the buckling resistance of a member in bending (see §4.3);

$M_{v,Ed}$ is the bending moment about v axis ($M_{v,Ed}=N_{Ed}(e_u+e_{initial})$);

$M_{v,Rd}$ is the design value of the resistance to bending moment about v-v axis (see §4.4);

k_{ij} are the interaction factors that are provided in Table 4.7;

ξ is a factor that depends on the cross-section class.

ANGELHY – Innovative solutions for design and strengthening of telecommunications **Page 34**
and transmission lattice towers using large angles from high strength steel and hybrid
techniques of angles with FRP strips

Table 4.7: Determination of k_{ij} factors

k_{ij} factors	
$k_{uu} = \dfrac{C_u}{1-\frac{N_{Ed}}{N_{cr,u}}}$ (4.32)	$k_{uv} = C_v$ (4.33)
$k_{vu} = C_u$ (4.34)	$k_{vv} = \dfrac{C_v}{1-\frac{N_{Ed}}{N_{cr,v}}}$ (4.35)
$C_u = 0{,}6+0{,}4\psi_u$ (4.36)	$C_v = 0{,}6+0{,}4\psi_v$ (4.37)
$-1 \leq \psi_u = \dfrac{M_{2u}}{M_{1u}} \leq 1$ (4.38)	$-1 \leq \psi_v = \dfrac{M_{2v}}{M_{1v}} \leq 1$ (4.39)

The ξ-factor depends on the cross-section class (Table 2.7). Its value ranges from 1 for elastic design, to 2 for plastic design, in dependence on the plate slenderness of the angle legs. More specifically it is:

$$c/t \leq 16\varepsilon: \qquad \xi = 2 \tag{4.40}$$

$$16\varepsilon < c/t < 26{,}3\varepsilon: \qquad \xi = \left[1 + \left(\frac{26{,}3\varepsilon - c/t}{26{,}3\varepsilon - 16\varepsilon}\right) \cdot (2-1)\right] \tag{4.41}$$

$$c/t > 26{,}3\varepsilon: \qquad \xi = 1 \tag{4.42}$$

4.5.1 Axial force and weak axis bending – Numerical validation

By considering only a constant weak axis moment along the member length caused by an eccentric axial force ($M_u=0$), the check equations transform to the following ones:

- <u>strong axis check</u>

$$\left(\frac{N_{Ed}}{N_{bu,Rd}}\right)^{\xi} + \frac{M_{v,Ed}}{M_{v,Rd}} \leq 1 \tag{4.43}$$

- <u>weak axis check</u>

$$\left(\frac{N_{Ed}}{N_{bv,Rd}}\right)^{\xi} + \frac{1}{1-\frac{N_{Ed}}{N_{cr,v}}} \cdot \frac{M_{v,Ed}}{M_{v,Rd}} \leq 1 \tag{4.44}$$

The details of the numerical samples that have been used, are presented in Table 4.8. The eccentricity is in u-u axis, and ranges between 5 and 35 mm; the value have been chosen randomly for each sample. All the analyses are for the tip in compression, which is more critical than the tip in tension.

Figure 4.9 presents the ratio between numerical and analytical load of the current proposal in dependence on the weak axis slenderness λ_v. The analytical load is determined by the maximum load that satisfies both equations (4.43) and (4.44), without safety factors. For all the samples, the weak axis check was the critical one.

ANGELHY – Innovative solutions for design and strengthening of telecommunications and transmission lattice towers using large angles from high strength steel and hybrid techniques of angles with FRP strips

Page 35

Table 4.8: Details for the samples subjected to an eccentric axial force causing a weak axis bending moment

| No	Cross-Section	L [mm]	f_y [N/mm²]	e_u [mm]	No	Cross-Section	L [mm]	f_y [N/mm²]	e_u [mm]
1		1000	355	10	17		2000	355	12
2	L 45x45x3	1000	460	10	18	L150x150x14	2000	460	12
3		2000	355	10	19		3000	355	20
4		2000	460	10	20		3000	460	20
5		1000	355	5	21		2000	355	10
6	L70x70x5	1000	460	5	22	L150x150x18	2000	460	10
7		2000	355	20	23		3000	355	32
8		2000	460	20	24		3000	460	32
9		1000	355	35	25		2000	355	8
10	L70x70x6	1000	460	35	26	L 250x250x17	2000	460	8
11		2000	355	35	27		3000	355	12
12		2000	460	35	28		3000	460	12
13		2000	355	25	29		2000	355	5
14	L 80x80x5	2000	460	25	30	L 250x250x22	2000	460	5
15		3000	355	25	31		3000	355	5
16		3000	460	25	32		3000	460	5
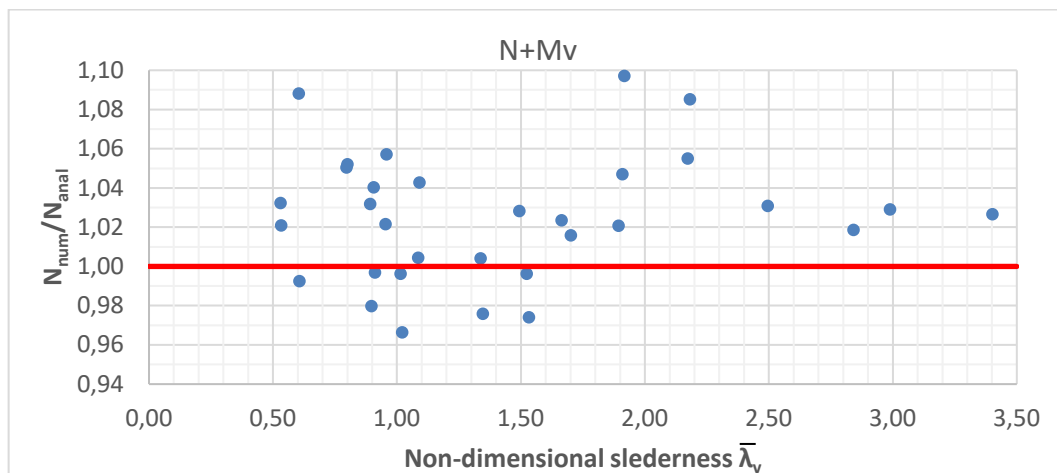
Figure 4.9: Ratio between numerical and analytical load for N+M_v

The mean value of the ratio N_{num}/N_{anal} is equal to 1,03 with a standard deviation of 3,2%. The analytical approach is validated quite well through the numerical results by accepting a 3% deviation.

4.5.2 Axial force and strong axis bending – Numerical validation

For an eccentric axial force combined with a constant strong axis moment along the member length, when $M_v=0$, the check equation becomes:

- strong axis check

$$\left(\frac{N_{Ed}}{N_{bu,Rd}} + \frac{1}{1-\frac{N_{Ed}}{N_{cr,u}}} \cdot \frac{M_{u,Ed}}{M_{u,Rd}} \right)^{\xi} \leq 1 \tag{4.45}$$

ANGELHY – Innovative solutions for design and strengthening of telecommunications **Page 36**
and transmission lattice towers using large angles from high strength steel and hybrid
techniques of angles with FRP strips

- <u>weak axis check</u>

$$\left(\frac{N_{Ed}}{N_{bv,Rd}} + \frac{M_{u,Ed}}{M_{u,Rd}}\right)^{\xi} \leq 1 \tag{4.46}$$

The details (profiles/lengths/steel grades) of the numerical samples that have been used, are the same with those presented in Table 4.8. The axial force is applied at the intersection point of minor principal axis v-v with the middle line of the leg thickness, and ranges between 14,57 and 84,00 mm, depending on the profile geometry.

(a) (b)
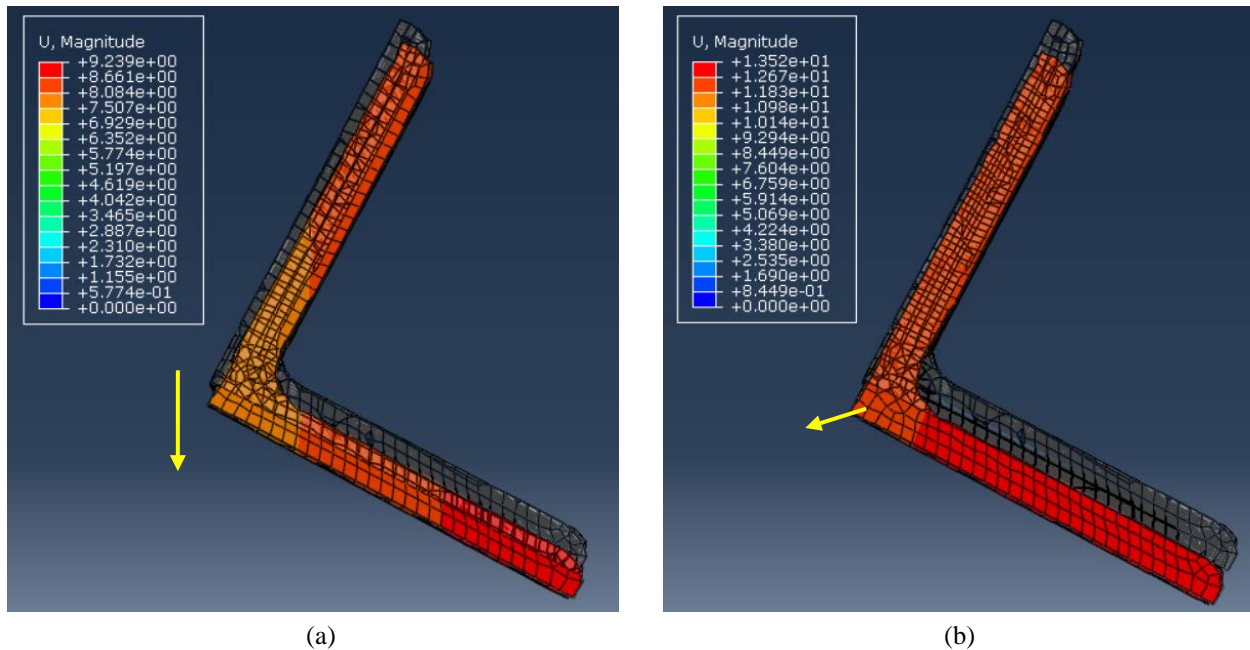
Figure 4.10: Movement of a profile subjected to an axial force and strong axis bending: (a) during loading-initial steps and (b) at the failure load
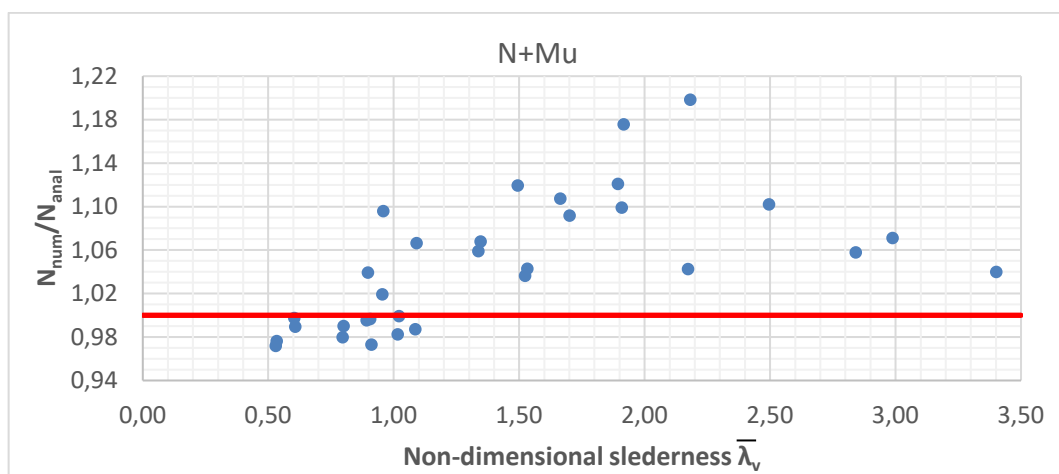
Figure 4.11: Ratio between numerical and analytical load for N+M$_u$

Figure 4.11 presents the ratio between numerical and analytical load of the current proposal in dependence on the weak axis slenderness λ_v. The analytical load is determined by the maximum load that satisfies both equations (4.43) and (4.44), without safety factors. For all the samples, the weak axis check was again the critical one. This can be explained by the fact that the member finally buckles

along weak axis. Analytically, lateral torsional buckling was ignored (χ_{LT} =1,0) due to one of the four conditions described in §4.3.1, and therefore the member buckles due to the axial load. Numerically, it can be shown from Figure 4.10 that the member starts to move laterally (along strong axis) but finally buckles along weak axis.

The mean value of the ratio N_{num}/N_{anal} is equal to 1,05 with a standard deviation of 5,9%, and the validation of the analytical approach is quite well by accepting a 3% deviation at the numerical results.

4.5.3 Axial force and bi-axial bending – Numerical validation

For angle members subjected to compression and bending, two checks for buckling around one or the other principal axis should be satisfied as they described by eq. (4.30) and (4.31). The details (profiles/lengths/steel grades) of the numerical samples that have been used, are the same with those presented in Table 4.8. The axial force is applied at the mid-height of the leg at the middle line of the leg thickness. This point could represent rather well the position of the connecting bolt for angles in structures.

Figure 4.12 presents the ratio between numerical and analytical load of the current proposal in dependence on the weak axis slenderness λ_v. The analytical load is determined by the maximum load that satisfies both equations (4.43) and (4.44), without safety factors. The weak axis check was the critical one for this loading case too, and the member buckles towards weak axis.
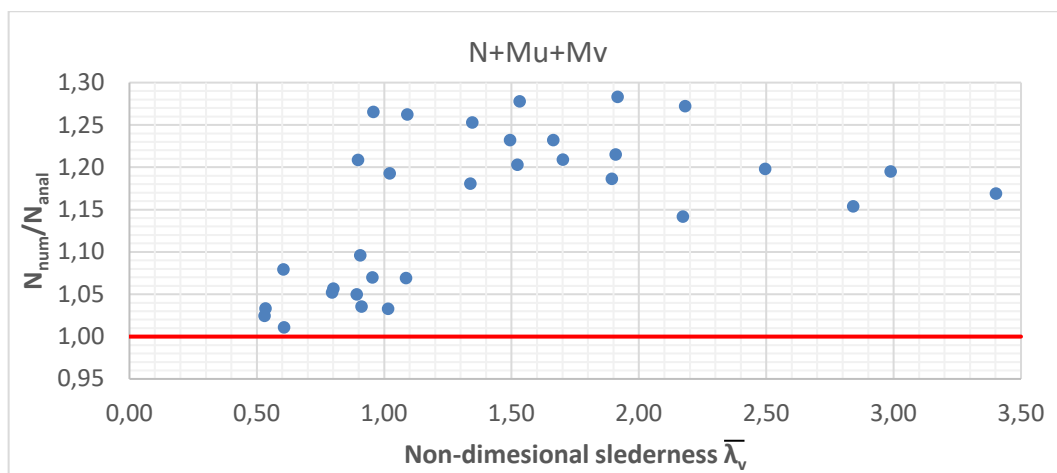
Figure 4.12: Ratio between numerical and analytical load for N+M$_u$+M$_v$

The mean value of the ratio N_{num}/N_{anal} is equal to 1,15 with a standard deviation of 8,8%. It can be seen that the analytical approach for the combined resistance is validated through the numerical results.

4.6 The General Method for equal leg angles

The general method applies to lateral and lateral torsional buckling for structural components with mono symmetric cross-sections, built-up or not, uniform or not, with complex support conditions or not, which are subject to compression and/or bi-axial bending in the plane, but which do not contain rotated plastic hinges. In this section, the general method is specified and presented for equal leg angle members, after it has been adjusted appropriately.

The out-of-plane buckling resistance of the member is sufficient if the following equation satisfies:

$$\chi_{op} \cdot \frac{a_{ult,k}}{\gamma_{M1}} \geq 1,0 \qquad (4.47)$$

where:

χ_{op} is the reduction factor corresponding to the non-dimensional slenderness $\overline{\lambda_{op}}$ and aimed at accounting for weak axis buckling only, as it has been shown from previous sections to be the predominate failure mode. Therefore, $\chi_{op} = \min\{\chi_u; \chi_v\}$. The selection of the buckling curve is based on [1].

$a_{ult,k}$ is the minimum load amplifier of the design loads to reach the characteristic resistance of the most critical cross-section of the structural component considering its in plane behaviour without taking lateral or lateral torsional buckling into account, but however accounting for all effects due to in plane geometrical deformation and imperfections, global and local, where relevant. It can be derived from eq.(4.48):

$$\frac{1}{\alpha_{ult,k}} = \frac{\sigma_{max}}{f_y} = \frac{\sigma_N}{f_y} + \frac{\sigma_{e_0}}{f_y} + \frac{\sigma_M}{f_y} \tag{4.48}$$

in which:

- the first term relates to the stress under pure compression;

- the second, to the second order maximum stress resulting from the amplification of the first order moment $N_{Ed} \cdot e_{0,EC3}$ ($e_{0,EC3}$ is the equivalent imperfection as defined in[1]), i.e. the moment $N_{Ed} \cdot e_{0,EC3}[1/(1-N_{Ed}/N_{cr,u})]$;

- the third one relates to the second order maximum stress resulting from the amplification of the first order moment $N_{Ed} \cdot e_v$ (e_v is the load eccentricity), which can be estimated as $N_{Ed} \cdot e_v[1/(1-N_{Ed}/N_{cr,u})]$.

The global relative slenderness $\overline{\lambda_{op}}$ for the structural component should be determined from eq.(4.49), in which the term $\alpha_{cr,op}$ is the minimum load amplifier for the design loads to reach the elastic critical load of the structural component associated to weak axis buckling.

$$\overline{\lambda_{op}} = \sqrt{\frac{\alpha_{ult,k}}{\alpha_{cr,op}}} \tag{4.49}$$

4.6.1 Numerical validation

The validation of the proposed method has been done through the numerical results obtained from the same analyses that have been performed in §4.5.3. Therefore, the axial force is applied at the mid-height of the leg at the middle line of the leg thickness.

Three cases were considered for the validation:

- Case 1:
  - "In-plane" 2nd order effects and bow imperfections are accounted for, in $a_{ult,k}$;
  - e_0 is taken from prEN1993-1-1:2019-§7.3.3.1 for relevant buckling curve (elastic verification);
  - elastic cross-section resistance is used (W_{el}).

- Case 2:
  - "In-plane" instability effects are considered as negligible;
  - 2nd order effects are disregarded ($k_u=1/(1-N_{Ed}/N_{cr,u})=1$) and e_0 is taken equal to zero (in recognition of the rather limited impact of this parameter);
  - probably such an assumption should be limited to angles connected by the leg;
  - in this case, the strong axis moment remains limited, as its influence;
  - elastic cross-section resistance is used (W_{el}).

- Case3:
  - Same assumptions as in Case 2, but taking into account the cross-section resistance using $W_u = \alpha W_{el,u}$, see eq. (3.8)-(3.11).

Figure 4.13 presents the ratio between numerical and analytical resistances obtained for the three different cases in dependence on the weak axis slenderness λ_v. The analytical resistance corresponds to the maximum load that satisfies equations (4.47). Each case is represented by a colour and the relative dot line is the trend line of the results using a 2nd order polynomial.

Table 4.9: Mean value and Standard deviation of the ratio N_{num}/N_{anal} for the deferent cases considered

Case	1	2	3
mean value	1,34	1,21	1,07
COV (%)	12,8	9,0	6,5
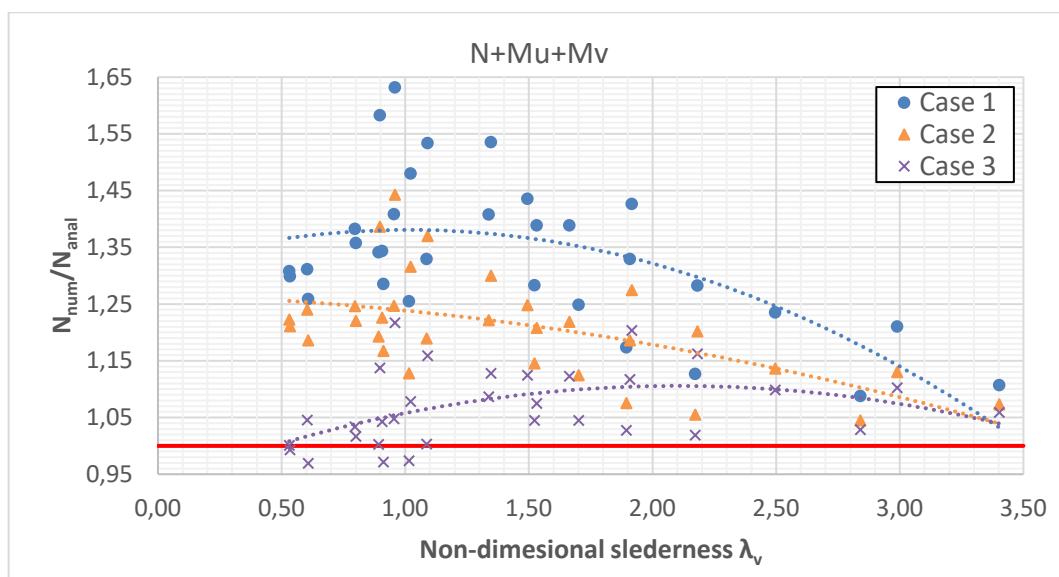
Figure 4.13: Ratio between numerical and analytical load, obtained through the general method, for N+M$_u$+M$_v$

The mean value and the standard deviation of the ratio N_{num}/N_{anal} is reported for each case in Table 4.9. It may be seen that the analytical approach for all the three cases is on the safe side (a 3% deviation at the numerical results is acceptable), with case 1 to be the safest. Therefore, each one may be used but the 3rd would be preferred.

5 The "leg-segment instability" mode

In task 1.2 of Work Package WP1 of the ANGELHY project [20], a not yet identified instability mode for lattice towers, that has been named "segment instability", has been observed and reported, through numerical simulations. These ones were based on the use of the full non-linear finite element software FINELG [17], using beam elements. Every single member had been properly modelled, in terms of orientation and eccentricities at its extremities and different types of analyses had been performed such as first and second order linear elastic analyses, an elastic instability analysis and second order plastic analyses.

A "segment instability" is defined as an instability mode associated to the buckling of more than one members forming a segment. As it is shown in Figure 5.1, in the present case the instability is associated to the buckling of the two diagonals of the leg, and therefore will be named as "leg-segment instability". The notations of the constitutive elements as well as the configuration of the tower's leg, are illustrated in Figure 5.3. The leg consists of three vertically orientated members: the main or

"exterior" leg and the two diagonals that are connected with a number of horizontal bars and bracing members forming "triangles". In fact, each of the two diagonals and the main leg member (exterior one) constituting the segment are stable individually and are able to resist to the applied maximum forces, as they have been initially designed to that. But the simultaneous buckling of the diagonals over the whole leg height, and involving a longitudinal rotation of the main leg member, represents a "new mode" which has been seen to be relevant in various usual design situations.
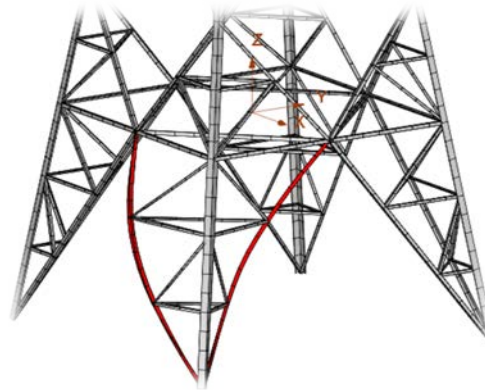
Figure 5.1: Elastic instability mode of the segment, observed in the transmission tower of [20]

Initial position
Deformed position
Displacement of the angle
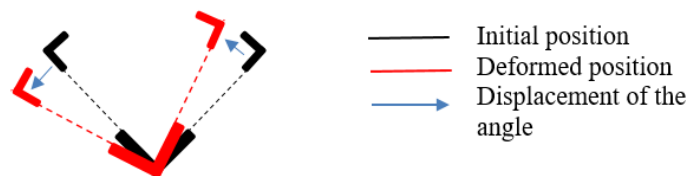
Figure 5.2: Deformation of the members through a horizontal cut in the leg

Horizontal level 1

Bracings right

Horizontal level 2

Horizontal level 3

Main leg

Diagonal 1 (left)
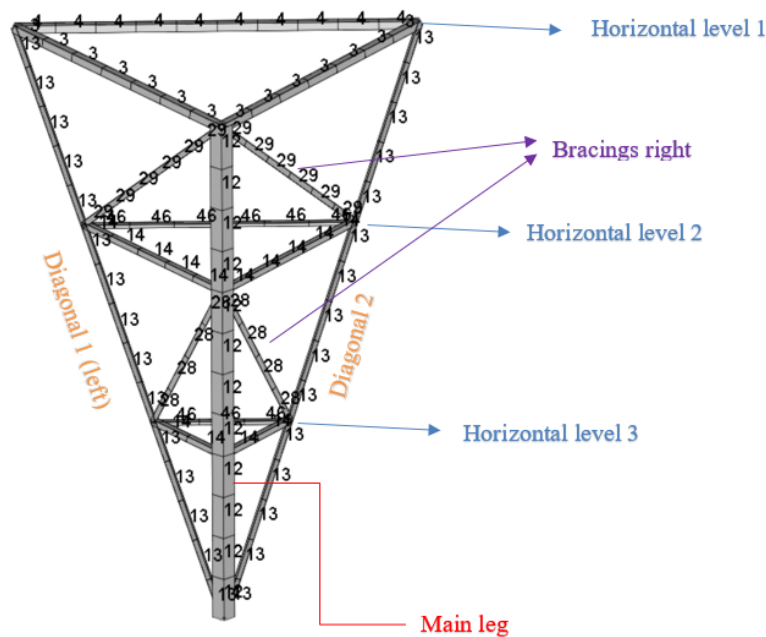
Diagonal 2

Figure 5.3: Notations of the constitutive elements of the leg of the tower

Figure 5.2 results from a horizontal cut in the leg and indicates how the constitutive elements deform in the instability mode. It is seen that:

- The diagonals move laterally and bends about an axis parallel to one of their angle legs.
- The main leg rotates about its longitudinal axis.
- The elements which "close the horizontal leg triangles" (not represented on the picture in Figure 5.2) do not undergo any deformation; they are just translated.

In the following, two design models and analytical formulas for the evaluation of the critical load of such a type of instability are presented, and validated numerically.

5.1 Proposed models for the segment instability

5.1.1 Simplified model

The equivalent model illustrated in Figure 5.4 has been built, in order to represent physically what is observed in the leg. The two parallel vertical members represent the two diagonals and the horizontal pinned members, the elements "closing the triangle". Both diagonals are assumed to be made of the same profile, as it happens mostly in practise. The extremities of the vertical members are assumed to be pinned; this is what is expected at the foundation level, while at the top, the very small restraining effect resulting from the actual continuity of the diagonals is neglected. The deformed shape of the system is seen on the right sketch (Figure 5.4).
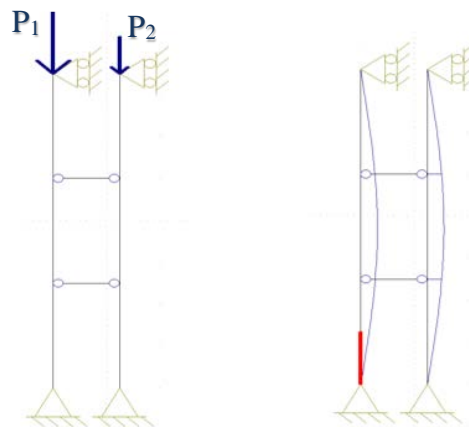
Figure 5.4: Equivalent model of the leg (left) and deformed shape (right)

For this simplified model, the critical load multiplier a_{cr} may be given by the following formula:

$$a_{cr} = \frac{2\pi^2 EI_y}{L^2.(P_1+P_2)} \tag{5.1}$$

where,

I_y is the moment of inertia about y-y geometrical axis (see Figure 1.1) of the diagonal's cross-section;

L   is the buckling length of the diagonal;

E   is the modulus of elasticity;

P_1, P_2 are the axial forces in the two diagonals.

It should be noted that this model is independent of the number of horizontal "rigid triangles", and therefore may be generally used for segments with pyramidal configuration.

5.1.2 Final model

In the previous proposed calculation model, the torsional stiffness of the exterior member is disregarded, what may be justified as a "safe" assumption.

ANGELHY – Innovative solutions for design and strengthening of telecommunications **Page 42**
and transmission lattice towers using large angles from high strength steel and hybrid
techniques of angles with FRP strips

But in this final proposed model (see §5.2.2 below), the beneficial effect of the torsional stiffness will be taken into account. And it will be considered that the axial force in the exterior member is not influencing its torsional stiffness. This may be justified by the following reasons:

- When the leg instability occurs, the exterior member is still assumed to be individually stable. If it is not the case, the individual buckling of the exterior member guides the failure and limit the pylon resistance, and so there is no need to try to evaluate the resistance of the leg which would lead to a higher critical load factor.

- The buckling of an individual member in compression follows overwhelmingly a flexural mode and not a torsional one.

When the leg instability develops, the exterior member is activated in torsion at the 1/3 and the 2/3 of the member length (L_{ext}). The first step consists in the evaluation of the torsional restraint offered by the rigidity of the exterior member in torsion.
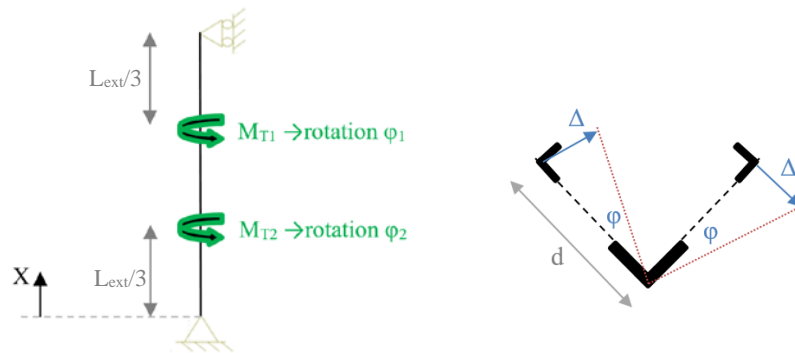
Figure 5.5: Schemes for the calculation for the torsional restraint brought by the exterior member

The torsional moment (see Figure 5.5) can be evaluated as follows, as far as M_{T1} and M_{T2} are equal:

$$\varphi = \int_0^{\frac{L_{ext}}{3}} \frac{M_T}{C} dx = \frac{M_T}{C} \cdot \frac{L_{ext}}{3} \quad \Rightarrow \quad M_T = \frac{3C}{L_{ext}} \varphi \tag{5.2}$$

The torsional rigidity C of the cross-section, is approximately equal to (see Figure 1.1 for the definition of h,t):

$$C = \frac{G}{3} \sum h b^3 = \frac{G}{3} \cdot 2 \cdot (h - 0.5t)t^3 \tag{5.3}$$

Then:

$$\left. \begin{array}{l} M_T = \frac{3C}{L_{ext}} \varphi \\ M_T = 2Fd \end{array} \right\} \Rightarrow \frac{3C}{L_{ext}} \varphi = 2Fd \xRightarrow{F=R\Delta} \frac{3C}{L_{ext}} \varphi = 2R\Delta d \xRightarrow{\Delta=d\varphi} \frac{3C}{L_{ext}} \varphi = 2Rd^2\varphi \tag{5.4}$$

where F is a force applied at each diagonal in direction of Δ and causes torsional moment at the exterior member of the leg ($M_T=2Fd$), while R is the lateral restraint of the diagonal ($R=F/\Delta$). By solving equation (5.4), the lateral restraint of the diagonal is:

$$R = \frac{3C}{2d^2 L_{ext}} = \frac{3C}{2L_{ext}} \cdot \frac{1}{d^2} \tag{5.5}$$

The torsional restraints evaluated at 1/3 or at 2/3 of the member length (where the rigid triangles act) are different (different values of d), what implies different values for M_{T1} and M_{T2} in Figure 5.5 and invalidates de facto the use of Formula (5.2). So, for sake of simplicity and in order to use the above formulae, the actual values of R at L/3 and at 2L/3 are substituted by a mean value of R_{mean} defined as follows:

$$R_{mean} = \frac{3C}{2L_{ext}} \cdot \frac{1}{n} \sum_{i=1}^{n} \frac{1}{d_i^2} \tag{5.6}$$

ANGELHY – Innovative solutions for design and strengthening of telecommunications **Page 43**
and transmission lattice towers using large angles from high strength steel and hybrid
techniques of angles with FRP strips

This is illustrated in Figure 5.6. To simplify it further, both restraints are merged into a single column. For the final model, which is finally selected (Figure 5.6-right drawing), the analytical expression can be found in literature [21] and is the following:

$$N_{cr} = \frac{\pi^2 EI}{L^2} + \frac{3}{16} K_T L \qquad \text{with} \quad K_T < \frac{16\pi^2 EI}{L^3} \tag{5.7}$$

If K_T reaches a value of $\frac{16\pi^2 EI}{L^3}$, the column will buckle in the second eigenmode (two half sine waves), with the result that further increases of the K_T values will not produce corresponding increases in the critical load. The column therefore effectively becomes restrained at its mid-height, and $N_{cr} = \frac{4\pi^2 EI}{L^2}$ (see Figure 5.7). In the specific case of the studied problem, the restraints remain quite low, and for sure much lower than $\frac{16\pi^2 EI}{L^3}$.
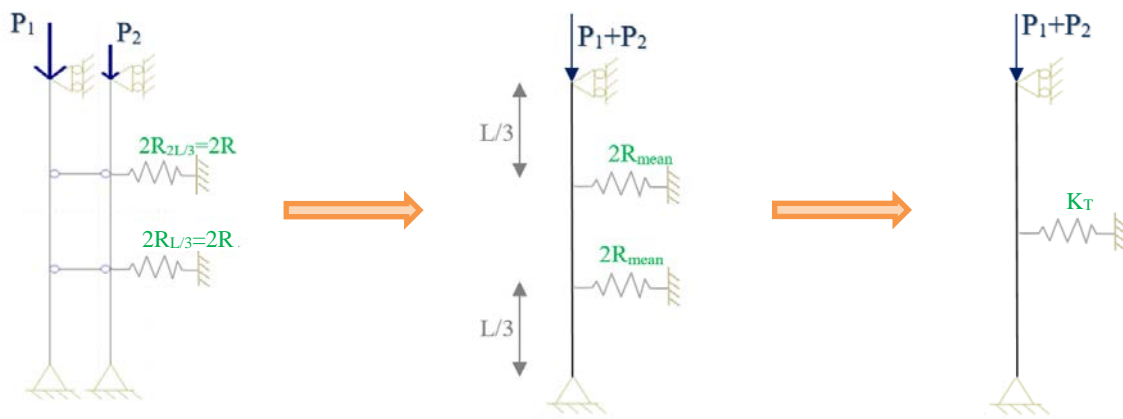
Figure 5.6: Initial (left), intermediate (middle) and final (right) proposed design model
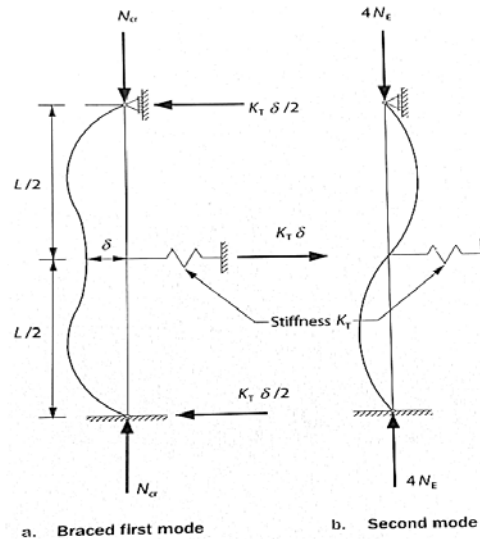
Figure 5.7: Column with a single discrete restrain-figure taken from ref. [22]

The determination of the spring stiffness K_T may be contemplated through a reference to the literature (p.474-475 of Ref. [9]), from which it may be deduced that for few discrete supports, the term $m\frac{C}{EI}l^3$ is constant. In this expression, m is the number of zones of length ($l = L/m$ separated by rigid triangles in the leg), $C=2R_{mean}$ and $EI =2EI_y$ where I_y is the value of the flexural rigidity of one diagonal.

$$m\frac{C}{EI}l^3 = const \quad \Rightarrow \quad m \cdot 2R_{mean} \cdot \left(\frac{L}{m}\right)^3 = 2 \cdot K_T \cdot \left(\frac{L}{2}\right)^3 \tag{5.8}$$

ANGELHY – Innovative solutions for design and strengthening of telecommunications   **Page 44**
and transmission lattice towers using large angles from high strength steel and hybrid
techniques of angles with FRP strips

This being, the equivalent spring stiffness K_T may be evaluated as follows:

$$K_T = \frac{4}{m^2}(2R_{mean}) \tag{5.9}$$

For the final model illustrated in Figure 5.6 (right sketch), the critical load multiplier a_{cr} is equal to:

$$a_{cr} = \frac{N_{cr}}{P_1+P_2} \tag{5.10}$$

where,

N_{cr} is the critical load of the equivalent column representing the segment;

P_1, P_2 are the axial applied forces in the two diagonals.

The critical load of the equivalent column can be evaluated by Eq.(5.11)

$$N_{cr} = \frac{\pi^2 EI_{y,tot}}{L^2} + \frac{3}{16}K_T L \tag{5.11}$$

where,

$I_{y,tot}$ is the total moment of inertia about y-y geometrical axis of both diagonals (i.e $I_{y,tot}=2I_y$);

L is the buckling length of the diagonal;

E is the modulus of elasticity;

K_T is the stiffness of the unique spring restraint, equals $\frac{4}{m^2}(2R_{mean})$;

R_{mean} can be evaluated through eq. (5.6);

m is the number of zones of length of the leg ($l = L/m$ separated by rigid horizontal triangles in the leg); the accuracy of the formulae for K_T is sufficient for a value of $m \leq 6$ (i.e for maximum 5 horizontal rigid triangles in the leg).

For both proposed models, the carrying capacity of the column may be evaluated through the Merchant-Rankine approach (see §5.2 – eq. (5.12)).

5.2 Numerical validations

The numerical validation of the proposed formulas (simplified and final) has been achieved initially through the 2D proposed models (models that illustrated in Figure 5.4 and Figure 5.6-right) by means of the OSSA2D software [22], and finally through the whole tower model, using FINELG software. The reference codes for the constitutive elements and the configuration of the tower leg simulated in FINELG, are illustrated in Figure 5.3, while the cross-section and the length of each member of the studied tower are reported in Table 5.1.

Table 5.1: Details of the members of the leg

Member	CS code	Cross-section	Length [m]
Diagonal 1 (left)	13	75x75x4	6,00
Diagonal 2 (right)	13	75x75x4	6,00
Main leg	12	150x150x13	5,00
Horizontal level 1	4	80x80x5	3,88
Horizontal level 1	3	80x80x5	2,74
Horizontal level 2	46	60x60x4	2,58
Horizontal level 2	14	60x60x4	1,83
Horizontal level 3	46	60x60x4	1,29
Horizontal level 3	14	60x60x4	0,91
Bracings left or right	29	60x60x4	2,29
Bracings left or right	28	60x60x4	1,78

ANGELHY – Innovative solutions for design and strengthening of telecommunications and transmission lattice towers using large angles from high strength steel and hybrid techniques of angles with FRP strips

Page 45

5.2.1 Simplified model

By using the OSSA2D software and performing an elastic buckling analysis, in which a force P_1=30 kN is applying and successively a force P_2 of 0, 5, 10, 15, 20, 25 and 30 kN, one finds the values of the critical load multipliers ($\alpha_{cr,OSSA2D}$) that reported in Table 5.2. The values ($\alpha_{cr,anal,1}$) obtained from equation (5.1) are reported in Table 5.2 too, and fits quite well with the OSSA2D results. Obviously, the simplified equivalent model disregards the rotational restraint of the main leg member as well as the continuity of the diagonals above the leg level.

Table 5.2: Results obtained through the OSSA2D and the analytical formula for the simplified model

P_1 [kN]	P_2 [kN]	$\alpha_{cr,OSSA2D}$ [-]	$\alpha_{cr,anal,1}$ [-]
30	0	1,19	1,21
30	5	1,02	1,03
30	10	0,89	0,90
30	15	0,80	0,80
30	20	0,72	0,72
30	25	0,65	0,66
30	30	0,59	0,60

Then, further numerical estimations of α_{cr} have been achieved for the transmission tower, subjected to different actual external load combinations so as to vary the loading on the leg (in the exterior member and in the two diagonals). In Table 5.3, the obtained numerical results ($\alpha_{cr,FIN}$) are compared with the analytical ones ($\alpha_{cr,anal,1}$) that have been evaluated by the proposed formula. The safe character of the simplified approach may be seen. Obviously, one should compare the ultimate resistances and not only the critical ones in order to put a definitive judgement on the level of safety of the approach.

Table 5.3: Results obtained through FINELG and the simplified analytical formula

Load combination	P_1 [kN]	P_2 [kN]	$\alpha_{cr,FIN}$ [-]	No of eigenmode	$\alpha_{cr,anal,1}$ [-]	α_{pl} [-]	$\alpha_{cr,anal,1}/\alpha_{cr,FIN}$ [-]	$\alpha_{cr,anal,1}/\alpha_{pl}$ [-]
G+W_y	30,00	0,00	1,37	1	1,21	13,639	0,881	0,0884
G+W_x	7,26	2,51	4,28	4	3,70	41,889	0,866	0,0884
G$_{tower}$	0,91	0,92	23,99	12	19,75	223,346	0,823	0,0884
W_x	5,78	1,37	6,42	1	5,06	57,227	0,788	0,0884
W_y	3,13	29,92	1,48	1	1,10	12,380	0,740	0,0884
Mean value	---	---	---	---	---	---	0,820	0,0884

In fact, a rough estimation of the carrying capacity of a column in compression can be done by the Merchant-Rankine approach:

$$\frac{1}{\alpha_u} = \frac{1}{\alpha_{cr}} + \frac{0,96}{\alpha_{pl}} \tag{5.12}$$

where α_{pl} can be evaluated by the following equation:

$$\alpha_{pl} = \frac{2 \cdot N_{pl}}{P_1 + P_2} \tag{5.13}$$

The results of α_{pl} are reported in Table 5.3 (N_{pl}=204,585 kN). By using the mean value of the ratio $\alpha_{cr,anal,1}/\alpha_{pl}$, it can be seen that the leg is rather slender: $\bar{\lambda} = \sqrt{\frac{\alpha_{pl}}{\alpha_{cr}}} = 3,363$. With so high slenderness values, the ultimate resistance of the leg is almost equal to its critical resistance (α_u=0,922α_{cr}). So, in this specific situation, even if the comparisons between the simplified model and FINELG would be done on the basis of the ultimate resistances, the safe character of the simplified approach would remain.

ANGELHY – Innovative solutions for design and strengthening of telecommunications   **Page 46**
and transmission lattice towers using large angles from high strength steel and hybrid
techniques of angles with FRP strips

5.2.2 Final model

For this model, first, the torsional rigidity C of the cross-section 150x150x13 is calculated and it is approximately equal to:

$$C = \frac{G}{3} \cdot 2 \cdot (h - 0{,}5t)t^3 = \frac{80769}{3} \cdot 2 \cdot (150 - 0{,}5 \cdot 13)13^3 = \boldsymbol{1{,}69761 \cdot 10^{10} \; Nmm^2}$$

Then, the mean value of the lateral restraint R of the diagonals is calculated, using eq. (5.6):

$$R_{mean} = \frac{3C}{2L_{ext}} \cdot \frac{1}{n} \sum_{i=1}^{n} \frac{1}{d_i^2} = \frac{3 \cdot 1{,}69761 \cdot 10^{10}}{2 \cdot 5000} \cdot \frac{1}{2}\left(\frac{1}{913^2} + \frac{1}{1827^2}\right) = 3{,}8177 N/mm$$

Consequently, **$2R_{mean}$=7,6354 N/mm**, and the stiffness of the spring is:

$$K_T = \frac{4}{m^2}(2R_{mean}) = \frac{4}{3^2}(7{,}6354) = \boldsymbol{3{,}393 \; N/mm}$$

A spring element has so been added in the OSSA2D model to restrain the system at L/2, with an axial stiffness equal to K_T. Then, an elastic buckling analysis, in which a force P_1=30 kN is applied together, successively, with a force P_2 of 0, 15, 20, and 30 kN, has been performed. The critical load multipliers ($\alpha_{cr,OSSA2D}$) as well as the values ($\alpha_{cr,anal,2}$) obtained from the analytical calculations are reported in Table 5.4, and are quite close.

Table 5.4: Results obtained through the OSSA2D and the analytical formula for the final model

P_1 [kN]	P_2 [kN]	$\alpha_{cr,OSSA2D}$ [-]	$\alpha_{cr,anal,2}$ [-]
30	0	1,320	1,334
30	15	0,895	0,889
30	20	0,806	0,800
30	30	0,672	0,667

Finally, the numerical results ($\alpha_{cr,FIN}$) that have been obtained for the transmission tower are compared with those obtained analytically ($\alpha_{cr,anal,2}$) in Table 5.5.

Table 5.5: Results obtained through FINELG and the final analytical formulae

Load combination	P_1 [kN]	P_2 [kN]	$\alpha_{cr,FIN}$ [-]	$\alpha_{cr,anal,2}$ [-]	α_{pl} [-]	$\alpha_{cr,anal,2}/\alpha_{cr,FIN}$ [-]	$\alpha_{cr,anal,2}/\alpha_{pl}$ [-]
G+W$_y$	30,00	0,00	1,37	1,33	13,639	0,973	0,0978
G+W$_x$	7,26	2,51	4,28	4,10	41,889	0,957	0,0978
G$_{tower}$	0,91	0,92	23,99	21,84	223,346	0,910	0,0978
Wx	5,78	1,37	6,42	5,60	57,227	0,872	0,0978
Wy	3,13	29,92	1,48	1,21	12,380	0,818	0,0978
Mean value	---	---	---	---	---	0,906	0,0978

With this improved version of the design model, the slenderness slightly changes ($\bar{\lambda} = 3{,}198$), but the leg remains rather slender. The ultimate resistance of the leg by Merchant-Rankine, is almost equal as for the simplified model, i.e α_u=0,914α_{cr}. Therefore, it is very important to estimate the value of α_{cr} with high accuracy so as to minimize the "error" in the calculations.

The final design model in which the rotational restraint of the main leg member is taken into account, gives better results than the simplified one, as it was expected. The results are closer to the reality, but are still on the safe side by approximately 9,4 %.

6 References

[1] prEN1993-1-1: Design of steel structures - Part 1-1: General rules and rules for buildings, Brussels, Comité Européen de Normalisation (CEN), 2019.

[2] Vayas I, Thanopoulos P, Vamvatsikos D, Vlachakis K, Dasiou ME, Bezas MZ, Jaspart JP, Demonceau JF, Proposal for design rules for single angle members, Research Report-ANGELHY project, National Technical University of Athens and University of Liège, 2019.

[3] ABAQUS, User's manual, Version 6.14, Simulia, 2014.

[4] EN 10056-2: Structural steel equal and unequal leg angles - Part 2: Tolerances on shape and dimensions, Brussels, Comité Européen de Normalisation (CEN), 1993.

[5] prEN1993-1-14 (20XX): XXXX, Brussels. Comité Européen de Normalisation (CEN), 2018.

[6] EN 50341-1: Overhead electrical lines exceeding AC 1 kV - Part 1: General requirements - Common specifications, 2012.

[7] EN1993-3-1: Design of steel structures - Part 3-1: Towers, masts and chimneys – Towers and masts, Brussels, Comité Européen de Normalisation (CEN), 2006.

[8] Eaton KJ, ESDEP-European Steel Design Education Programme, 3rd Nordic conference on computer aided learning, Finland, ISBN 9512207311, Helsinki University of Technology, 1991.

[9] Petersen C, Statik und Stabilität der Baukonstruktionen (in German), ISBN 978-3-528-18663-0, Friedrich Vieweg & Sohn Verlag, Germany, 1982.

[10] Gardner L, Fieber A, Macorini L, Formulae for Calculating Elastic Local Buckling Stresses of Full Structural cross-sections, Structures, Vol.17, pp. 2-20, 2019.

[11] EN1993-1-5: Design of steel structures - Part 1-5: Plate structural elements, Brussels, Comité Europeen de Normalisation (CEN), 2006.

[12] Greiner R, Lechner A, Kettler M, Jaspart JP, Weynand K, Oerder R, Dehan V, Valorisation action of plastic member capacity of semi-compact steel sections: A more economic design (SEMI-COMP+), RFCS European Research project, Directorate-General for Research and Innovation (European Commission), ISBN 978-92-79-29312-2, 2013.

[13] EN 1090-2: Technical requirements for the execution of steel structures, Comité Européen de Normalisation (CEN), 2008.

[14] prEN 1993-1-14 (20XX): XXXX, Brussels. Comité Européen de Normalisation (CEN), 2018

[15] Zhang L, Jaspart JP, Stability of members in compression made of large hot-rolled and welded angles, Research Report, University of Liège, 2013.

[16] Moze P, Cajot LG, Sinur F, Rejec K, & Beg D, Residual stress distribution of large steel equal leg angles. Engineering Structures, Vol.71, 35-47, 2014.

[17] FINELG: Non-linear finite element analysis program, User's manual, Version 9.0, Greisch Ingeniere, 2003.

[18] de Ville de Goyet V, L'analyse statique non linéaire par la méthode des éléments finis des structures spatiales formées de poutres à section non symétrique, PhD thesis, University of Liège, 1989.

[19] EN1993-1-1: Design of steel structures - Part 1-1: General rules and rules for buildings, Brussels, Comité Européen de Normalisation (CEN), 2005.

[20] Bezas MZ, Jaspart JP, Demonceau JF, Tibolt M, Deliverable 1.3: Report on analysis and design of 6 case studies, Research Report-ANGELHY project, University of Liege, 2019.

[21] Gardner L, Stability of steel beams and columns in accordance with Eurocodes and UK National Annexes, SCI publication P360, ISBN 978-1-85942-199-4, Berkshire, UK, 2011.

ANGELHY – Innovative solutions for design and strengthening of telecommunications **Page 48**
and transmission lattice towers using large angles from high strength steel and hybrid
techniques of angles with FRP strips

[22] OSSA2D: Finite element analysis program, User's manual, Version 3.4, University of Liege, 2020.

List of Figures

ANGELHY – Innovative solutions for design and strengthening of telecommunications and transmission lattice towers using large angles from high strength steel and hybrid techniques of angles with FRP strips

Page 49

List of Tables